CONTROLS OF BASEMENT FABRIC ON RIFT COUPLING AND DEVELOPMENT OF NORMAL FAULT GEOMETRIES: INSIGHTS FROM THE RUKWA – NORTH MALAWI RIFT

Erin Heilman[1]

Folarin Kolawole[2]

Estella A. Atekwana[3]*

Micah Mayle[1]

Mohamed G. Abdelsalam[1]

[1]*Boone Pickens School of Geology*
Oklahoma State University
Stillwater, Oklahoma, USA

[2]*ConocoPhillips School of Geology & Geophysics*
University of Oklahoma
Norman, Oklahoma, USA

[3]*Department of Geological Sciences*
College of Earth, Ocean, and Environment
University of Delaware
Newark, Delaware, USA

Corresponding author email: atekwana@udel.edu

August 2018

Highlights

- To the SW, newfound strike-slip fault links the Rukwa and North Malawi Rift (RNMRS)
- To the NE, RNMRS border faults, intervening faults and volcanic centers are colinear
- RNMRS border faults and transfer structures align with pre-existing basement fabrics
- Basement fabrics guide the development of normal fault geometries and rift bifurcation
- Basement fabrics facilitate the coupling of the RMRS border faults and transfer structures

ABSTRACT

The Rukwa Rift and North Malawi Rift Segments (RNMRS) both define a major rift-oblique segment of the East African Rift System (EARS), and although the two young rifts show colinear approaching geometries, they are often regarded as discrete rifts due to the presence of the intervening Mbozi Block uplift located in-between. This problem has been complicated by the dominance of the Rungwe volcanic features along the northeastern boundary of the Mbozi Block and lack of distinct normal faults along the southwestern boundary of the block. Here, we investigate the coupling of discrete rift segments during the onset of continental rifting, modulated by the control of pre-existing basement fabrics on the development of the border fault geometries and linkage across the intra-rift transfer zone. We utilized the Shuttle Radar Topography Mission Digital Elevation Models (SRTM-DEM) to investigate the morphological architecture of the rift domains; and aeromagnetic data and SRTM-DEM to assess the relationships between the rift structures and the pre-existing basement fabric (in plan-view). Our results show that the present-day morphology of the RNMRS is characterized by along-rift alternation of rift shoulder polarity, characteristic of coupled rift segments. Careful interpretation

96   of filtered aeromagnetic maps along the northeastern and southwestern boundaries of the

97   RNMRS reveal striking alignment of the rift-bounding faults with colinear NW-SE-trending pre-

98   existing basement fabrics. We find that rift coupling along the northeastern boundary of the

99   Mbozi Block transfer zone is accommodated by magmatism utilizing pre-existing fault systems,

100   whereas, coupling along the southwestern boundary is accommodated by a new-found dextral

101   strike-slip fault. Additionally, we show how the configuration of the pre-existing basement

102   fabrics may influence the development of rectilinear or curvilinear normal fault geometries

103   (plan-view) along the rifts, and the formation of basin-scale rift bifurcation around basement

104   inter-rift transfer zones. In summary, we suggest that the structural continuation of the boundary

105   faults along the RNMRS, and their alignment with colinear basement fabrics demonstrate the

106   influence of structural inheritance on the coupling and amalgamation of approaching rift

107   segments.

108

109

110

111

112

113

114

115

116

117

118

1. INTRODUCTION

Pre-existing basement fabrics are often major facilitators of continental rifting environments. Mechanically, they represent areas of structural weakness that can become reactivated and allow rifts to propagate preferentially along them (e.g., Daly et al., 1989). Several studies have documented the relationships between rift faults and the pre-existing basement fabrics (e.g., Wheeler and Karson, 1989; Kinabo et al., 2007, 2008; Taylor et al., 2011; Phillips et al., 2016; Kolawole et al., 2018; Siuda et al., 2018). Further, recent studies have assessed the 3-dimensional relationship between pre-existing basement thrusts and intra-rift normal faults, revealing the control of the pre-existing basement structures on the nucleation and strain distribution along the normal faults (e.g., Collanega et al., 2018). In the Cenozoic East African Rift System (EARS), which is divided into an Eastern, a Western and a Southwestern Branch (Fig. 1A), several zones of well-developed basement fabric influence rifting. One of the best recently-documented examples highlighting the influence of the Precambrian basement shear zones on rifting in eastern Africa is the role of the Mwembeshi Shear Zone on the development of the Luangwa Rift (Fig. 1A; Sarafian et al., 2018). It was demonstrated that the Mwembeshi Shear Zone acted as lithospheric conduit for fluids to migrate up the lithosphere, thus facilitating the weakening and subsequent initiation of the Luangwa rift in the Permo-Triassic.

However, the relationship between rift segments along the western branch of the EARS and the Precambrian shear zones is rather complex and warrants detailed and careful examination. For example, the Precambrian NW-trending Aswa shear zone resulted in the termination (rather than facilitation) of the northeastward propagation of the Albertine-Rhino graben which represents the northern-most segment of the Western Branch (Katumwehe et al., 2015) (Fig. 1A). On a basin scale, previous studies have also shown that pre-existing basement

142 shear zones can influence the localization of fault development (e.g., Phillips et al., 2016;

143 Kolawole et al., 2018), and in fact control fault segmentation and across-basin strain transfer at

144 later stages of rift development (e.g., Muirhead and Kattenhorn, 2018).

145 The border faults along large continental rift systems, e.g., the EARS, are typically ~100

146 km long (e.g., Foster et al., 1997; Lao-Davila et al., 2015), and the development of such large

147 normal faults with complex segment linkage styles are yet to be fully understood (e.g., Fossen

148 and Rotevatn, 2016; Gawthorpe et al., 2003; Rotevatn et al., 2018). However, since the

149 interactions between the large normal faults within juvenile extensional tectonic settings lead to

150 the systematic coupling of rift segments across transfer zones (e.g., Corti, 2012), border fault

151 segmentation, geometries and continuity between rift segments can provide insight into the

152 larger process of coupling between the segments of a rift system.

153 In this study, we focus on the Rukwa-North Malawi segment of the EARS, which is a

154 major rift-oblique segment of the rift system and serves as the central segment of the system. For

155 simplicity, we here-in refer to the Rukwa - Northern Malawi Rift segment of the East African

156 Rift as the "RNMRS". This segment is composed of the Rukwa Rift basin, the North Malawi

157 Rift basin and the Mbozi Block which represents the accommodation zone between the two rifts

158 (Fig. 1B). We address the longstanding question of the role of long-lived pre-existing basement

159 structures in the development of the trends and geometries of rift-bounding faults, leading to

160 subsequent coupling of individual rift segments during the onset of continental rifting. We

161 demonstrate that there is continuous structural connectivity along the boundaries of the RNMRS,

162 modulated by reactivation of the Precambrian metamorphic fabrics, and show that the

163 characteristic plan-view geometries of the rift-bounding faults are modulated by the

164 configuration of the basement fabric.

2. GEOLOGIC SETTING

2.1. The Precambrian Domains

The Rukwa-North Malawi Rift Segment is located within the NW-trending Paleoproterozoic Ubendian orogenic belt which is sandwiched between the Archean Tanzanian craton in the northeast and the Bangweulu cratonic block to the southwest (Figs. 2A-B; Fritz et al., 2013). The Ubendian Belt is composed of different Precambrian terranes bounded by steep shear zones (Delvaux et al., 2012). These terranes contain granulite-facies metamorphic rocks (2100-2025 Ma), amphibolite-facies metamorphic rocks and granitoids (1960-1800 Ma) that have undergone dextral strike-slip shearing and granitic plutons (1090-1120 Ma), (Fritz et al., 2013). The Paleoproterozoic Usagaran orogenic belt that extends NE-SW perpendicular to the Ubendian orogenic belt in southern Tanzania, is composed of eclogites (~2000 Ma), volcano-sedimentary cover with some low-grade metamorphism (~1920 Ma), and granitoids and granitoid gneisses (1900-1730 Ma) (Fritz et al., 2013). The Usagaran and Ubendian orogenic belts resulted from collision with the Tanzania craton, where the Usagaran orogenic belt was thrust onto the craton and the Ubendian orogenic belt was accreted along the craton's margin because of strike-slip motion (Daly, 1988; Lenoir et al., 1994). The Ubendian Belt was reactivated several times, first at ~1860 Ma as a shear zone, then again at ~800 Ma and was subsequently reactivated about every 200 Ma (Lenoir et al., 1994). Mapped shear zones along the Ubendian Belt include the ~600 km long and ~30 km-wide Mughese Shear Zone, the Mtose Shear Zone, and the Chisi Shear Zone (Fig. 2; Daly, 1988; Schenk et al., 2006; Delvaux et al., 2012). Recent studies have highlighted the role of the Mughese Shear Zone in fault development and the distribution of seismicity in Northern Malawi Rift Basin (Dawson et al. 2017; Kolawole et al., 2018).

2.2. The Rukwa Rift, Northern Malawi Rift, and the Mbozi Block accommodation zone (RNMRS)

The RNMRS evolved during the Permo-Triassic episode of rifting that affected southern and eastern Africa, also known as Karoo rifting (Chorowicz, 2005). Outcrops of Karoo sediments have been mapped along the southern end of the Rukwa Rift (Figure 2) and the northern section of the North Malawi Rift Basin (Kilembe and Rosendahl, 1992). These sediments lie unconformably over the Precambrian basement and consist mainly of sandstone, shale, and coal and thicken towards the border faults providing evidence for reactivation of synthetic faulting in the Permo-Triassic (Morley, 1992; Delvaux et al., 1992).

Cenozoic rifting began in the Upper Miocene, characterized by normal faulting and basin subsidence with the diagenesis of Red Sandstones and Lake Bed Sediments (Delvaux and Hanon, 1991). Additional subsidence occurred after the deposition of these packages, and in different directions, evidenced by the drag orientations of sediment packages on the faults (Kilembe and Rosendahl, 1992). The Cenozoic rifting featured the reactivation of older faults as seen in seismic profiles of the Rukwa Rift in which the faults are mostly contiguous from Karoo sediments to Red Sandstones to Lake Beds (Kervyn et al., 2006). The present-day tectonic activity in the RNMRS consists of limited volcanic eruptions, minor seismicity in the Mbozi Block region, and continued sedimentation in the Rukwa and North Malawi basins (Delvaux and Hanon, 1991).

The present-day architecture of the RNMRS consists of the Rukwa Rift to the northwest of the segment, with the Lupa Fault (generally considered the border fault) bounding it to the northeast and the Ufipa Fault to the SW (Fig. 1B). Towards the southeastern end of the Rukwa Rift. It bifurcates around the Mbozi Block forming the Songwe Trough (ST) to the northeast and the Musangano Trough (MT) to the southwest. The Mbozi Block transitions into the North

211   Malawi Rift (also known as the North Basin) which represents the southeastern end of the

212   RNMRS and it consists of a half-graben, bounded to the northeast by the Livingstone Fault (Fig.

213   1B). The Mbozi Block is referred to as an accommodation zone because it is thought to

214   accommodate and transfer relative strain between the Rukwa and North Malawi Rift Basins

215   (Delvaux and Hanon, 1993)

216   The Mbozi is a mass of Precambrian basement that is composed of Meta-basites and

217   intermediate granulites and quartzites of the Mbozi Terrane (Daly, 1988) and is bounded to the

218   southwestern by the Mughese Shear Zone (Fig. 2B), and overlain on the northeast by the

219   volcanic deposits of the Rungwe Volcanic Province (RVP). The RVP is a ~1500 km^2 area of

220   volcanic rocks and structures that evolved ca. 9 Ma (e.g., Fontijn et al., 2012), and a strong

221   tectonic control on the localization of volcanic centers have been inferred (e.g., Fontijn et al.,

222   2010, 2012). To the northeast of the RVP, a poorly defined NE-trending rift basin occurs, known

223   as the "Usangu Basin", where Permo-Triassic to Recent sedimentary rocks overlie the

224   Precambrian basement (Mbede, 2002).

225   The crustal thickness beneath the Rukwa Rift is ~37.5 km (Kim et al., 2009), but varies

226   between ~33 km and ~39 km along the rift shoulder (Ufipa Plateau) (Hodgson et al., 2017), and

227   increases slightly to 41.1–42.1 km in the northwestern-most part of the rift where the rifting is

228   minimal. These suggest that overall, the crustal thinning beneath the rift has been minimal but

229   may be slightly more beneath the Songwe Trough (Njinju et al., 2018). Camelbeeck and Iranga

230   (1996) estimated ~42 km crustal thickness beneath the Songwe Trough. Whereas, an average

231   crustal thickness of 39 km has been estimated for the Rungwe Volcanic Province, ~37-39 km for

232   the North Malawi Rift, and 38-42 km for the Proterozoic terrains surrounding the North Malawi

233   Rift (Borrego et al., 2016; Njinju et al., 2018).

234 *2.3. Kinematics of the RNMRS*

235 The mode of opening of the Rukwa Rift – Northern Malawi Rift segment is controversial.

236 Overall, two models have been proposed. One of the models advocates for orthogonal rifting due

237 to the dominance of NW-trending pre-existing basement fabric in the region, which resulted in

238 the rotation of the E-W directed regional extension into NE-SW, thus producing NW-striking

239 normal faults (e.g., Delvaux et al., 1992; Morley, 2010; Delvaux et al., 2012). The other model

240 argues for oblique extension primarily due to the obliqueness of the rift segment to the E-W

241 directed extension, thus resulting in the development of NW-trending dextral strike-slip faults

242 (e.g., Chorowicz, 1989; Daly et al., 1989; Wheeler and Karson, 1994; Kervyn et al., 2006;

243 Mortimer et al., 2007). Both models are based on observations from only the Rukwa Rift and

244 North Malawi Rifts, and did not consider the kinematics of brittle structures along the Mbozi

245 Block accommodation zone.

246

247 **3.0 MATERIAL AND METHODS**

248 In this study, we carried out detailed mapping of exposed and buried fault segments within the

249 RNMRS. We utilized Shuttle Radar Topography Mission (SRTM) Digital Elevation Model

250 (DEM) to locate surface expressions of faults; and filtered aeromagnetic data to map the plan-

251 view trace of basement faults and metamorphic fabrics.

252

253 *3.1. SRTM DEM Data*

254 We extracted topographical profiles along the length of the rift from the SRTM DEM data to

255 investigate surface morphology of the rift segments which could provide insight into the

256 evolving nature of the rift architecture along the RNMRS.

3.2. Aeromagnetic Data

We combined three separate aeromagnetic surveys consisting of data acquired over northeastern Zambia, southern Tanzania and Northern Malawi. The Tanzania survey was collected between 1977-1980 with flight height of 200 m and a flight line spacing of 1 km. The Zambia survey was collected between 1973-1976 with a flight height of 150 m and a flight line spacing of 800-1000 m. The Malawi survey was carried out in 2013 with a flight height of 80 m, a flight line spacing of 250 m. Before merging the three surveys, we first corrected for the skewness of the data by reducing each of them to the magnetic pole (RTP). The RTP correction normalizes the magnetic field to the magnetic field at the pole so the anomalies retain their correct strike and shape, allowing the magnetic data to be interpreted as geologic structures (Baranov, 1957; Silva, 1986). Afterwards, we applied upward-continuation (Henderson and Zeitz, 1949) of 120 m to the RTP-corrected Malawi data, 50 m to the Zambia data in order to mathematically normalize the three datasets to a 200 m observational height. We then merged the three surveys into a single aeromagnetic grid file. Further, we applied the vertical derivative (VDR) filter to the merged data in order to enhance magnetic gradients associated with possible basement faults and basement metamorphic fabrics (Salem et al., 2008).

The vertical derivative edge filter has been very effective in the mapping of plan-view trace of buried active faults from aeromagnetic data in different parts of the EARS (Kinabo et al., 2007, 2008; Kolawole et al., 2017, 2018). Excluding the Rungwe Volcanic Province (RVP; Figure 3) where volcanic materials overlie the crystalline basement, there is no information on the presence of basaltic rocks along the fault segments interpreted in this study. Therefore, we assume induced magnetization as the primary source of magnetization, except in the Rungwe Volcanic Province (RVP) where volcanic deposits are present. However, we do not have

280   information on remanent magnetization in the RVP at this time. Due to the higher spatial

281   resolution of the Malawi aeromagnetic data (62 m grid cell size) compared to those covering

282   Zambia (225 m grid cell size) and Tanzania (250 m grid cell size), the magnetic anomalies are

283   most significantly better resolved in the Malawi part of the filtered aeromagnetic maps.

284

285   **4.0 RESULTS**

286   *4.1. Variation in rift morphology from topographic profiles*

287   We examined fifteen rift-orthogonal topographic profiles (spaced at 40 km) along the RNMRS

288   (Fig. 1B) to understand the overall along-strike variation in rift morphology. The investigation of

289   rift dynamics by careful analyses of the topographic structures has provided important

290   information on the subsurface architecture of rift systems (e.g., Pik et al., 2008; Wichura et al.,

291   2011; Lao-Davila et al., 2015). Our morphological assessments focus on the variation in the

292   scarp-heights (relief above the surface) of exposed normal faults along the RMNRS. This

293   provides the minimum estimate of the relative vertical displacements of the faults at the point of

294   assessment, hence the term 'exposed minimum vertical displacement' (EMVD) (Lao-Davila et

295   al., 2015).

296   Profile 1 (Fig. 3), obtained at the northern tip of the Rukwa Rift shows no pronounced

297   fault scarps, and the slight topographic high between Lake Tanganyika and Ufipa Fault

298   represents the northernmost tip of the Ufipa Plateau. In Profile 2, the surface morphology of the

299   rift shows sharp topographic gradients bounding the Rukwa Rift Valley. These topographic

300   gradients correspond to the scarps of the Ufipa Fault (600 m) and the Lupa Fault (750 m). In this

301   northern part of the Rukwa Rift, the Ufipa and Lupa Faults have comparable scarp heights, thus

302   illustrating a typical graben structure. In Profile 3, the rift structure changes into a half-graben

12

303 surface morphology with the Ufipa Fault having a significantly higher escarpment than the Lupa

304 Fault (~900 m difference). Profiles 4 to 7 show the same half-graben morphology for the Rukwa

305 Rift as in Profile 3; however, we observe that the Ufipa Fault scarp is much higher than the

306 topography of the Ufipa Plateau to its west along Profile 4.

307 Along Profiles 6 and 7, we observe that the Ufipa Fault scarp is lower than in the

308 northern profiles (Profiles 1-5) and that the Lupa Fault scarp is also higher than in the northern

309 profiles. In Profile 7, the Rukwa Rift splits into two basins separated by the Mbozi Block such

310 that the west basin (Musangano Trough) is bound by the Ufipa Fault to the southwest, and the

311 east basin (Songwe Trough) is bound by the Lupa Fault to the northeast. Profiles 7 to 9 shows a

312 continuous southeastward decrease in the scarp heights of the Ufipa and Lupa Faults; and

313 although the Ufipa Fault scarp is still visible south of the Mbozi Block along Profile 9, the Lupa

314 Fault scarp is significantly diminished. Profile 9 shows a gentle topographic transition from the

315 Musangano Trough to the Mbozi Block, but to the northeast of the Mbozi Block, the topography

316 spikes abruptly, representing the northern limits of the Rungwe Volcanic Province (RVP). In

317 Profile 10, the Ufipa Fault bounds what appears to be the southernmost extent of the Musangano

318 Trough, while the uplifted Mbozi – RVP domain dominates the terrain and drops off into the

319 Usangu Trough to the northeast. Profile 11 transects the northernmost tip of the North Malawi

320 Rift, where the RVP (bounded to the northeast by the Livingstone Fault scarp) represents the

321 most dominant structure in the terrain and the entire topography of the Mbozi Block and areas to

322 its southwest are relatively lower.

323 Profiles 12 and 13 illustrate half-graben morphologies for the North Malawi Rift (North

324 Basin) with the Livingstone Fault (northeast bounding fault) dominating the topography. Profile

325 14 transects the transfer zone between the North and Usisya Basins of the Malawi Rift showing

326 both the Livingstone border fault to the northeast and the Nyika Plateau to the southwest. Profile

327 15 which transects the Usisya Basin describes a half-graben surface morphology but in which the

328 rift bounding fault is located on the southwest.

329

330 *4.2. Aeromagnetic lineaments and basement fabric*

331 The RTP merged (Fig. 4A) and edge-enhanced (Fig. 4B) aeromagnetic maps over the RNMRS

332 provide a continuous plan-view image of the basement structures along the rift segment.

333 Although the Malawi part of the merged data has the highest resolution, the moderate resolution

334 of the Tanzania and Zambia parts of the data allows for considerable delineation of the trends of

335 magnetic anomalies. Overall, the areas of basement exposures exhibit high amplitude, high

336 frequency and short wavelength magnetic anomalies that delineate lineaments of interpretable

337 trends (e.g., Kolawole et al., 2018). The high frequency lineaments can be easily observed on the

338 rift shoulders of the Rukwa and North Malawi Rifts (Fig. 4B), and are commonly truncated at the

339 rift margins by the rift-bounding faults (black arrows in Fig. 4B).

340   Within the rift valleys where sedimentary rocks overlie the deeply-buried basement

341 rocks, the detailed magnetic fabric of the basement becomes suppressed such that gradients in

342 the magnetic data could correspond to fault offset within the magnetic source (e.g., Grauch and

343 Hudson, 2007, 2011; Kolawole et al., 2018) or remnants of the suppressed magnetic foliation of

344 the source (Kolawole et al., 2018). In the study area, the magnetic anomalies within the rift

345 basins are dominated by relatively lower amplitude, longer wavelength and lower frequency

346 anomalies.

347

348

14

349 *4.3. SRTM DEM Fault trends and Aeromagnetic lineaments*

350 We compare the along-axis geometry of the rift-bounding faults (from SRTM DEM) with the

351 metamorphic fabric (in plan view) of the host basement rocks along the rift shoulders (from

352 filtered aeromagnetic data) (Figs. 5-11). Figures 5-9 focus on the southwestern boundary of the

353 RNMRS, consisting of the Ufipa Fault of the Rukwa Rift, the southwestern boundary of the

354 Mbozi Block and the southwestern boundary faults of the North Malawi Rift. Whereas, Figures

355 10 and 11 focus on the northeastern boundary of the RNMRS, consisting of the Lupa Fault of

356 Rukwa Rift, the northeastern boundary of the Mbozi Block (i.e. the Rungwe Volcanic Province)

357 and the Livingstone Fault of the North Malawi Rift. We constrain our identification of the

358 Precambrian terranes and strike of their fabrics with previous field studies of the Precambrian

359 basement along the RNMRS (e.g., Daly, 1988; Wheeler and Karson, 1989; Lenoir et al., 1994;

360 Theunissen et al., 1996; Boven et al., 1999; Fernandez-Alonso et al., 2001; Ring et al., 2002;

361 Schenk et al., 2006; Delvaux et al., 2012, Lawley et al., 2013; Kolawole et al., 2018). Overall,

362 within the study area, we observe that the basement fabrics exhibit two styles, (1) discrete fabrics

363 which include isolated magnetic lineaments of strong amplitude; and (2) distributed fabrics

364 which encompass fabric sets of multiple medium-to-low amplitude magnetic lineaments as

365 distributed fabrics.

366

367 *4.3.1. Southwestern boundary of the RNMRS*

368 In the northernmost part of SW Rukwa Rift (Chisi area) (Figs. 5A-C), we observe curvilinear

369 fault geometries that follow Precambrian fabric (e.g., Ufipa, Chisi, Kalambo and Kanda Faults).

370 In the Chisi area, the Rukwa Rift border fault consists of the Northern Ufipa Fault segment and

371 the Chisi Fault segment. The tip of the Northern Ufipa Fault segment terminates against the

372   WNW-ESE Chisi Fault at a high angle (Fig. 5A). The Chisi Fault aligns with a strong WNW-

373   ESE magnetic-high lineament (discrete fabric) (Fig. 5B-C) known as the Chisi Shear Zone,

374   which extends eastward into the rift basin (Theunissen et al., 1996; Boven et al., 1999; Schenk et

375   al., 2006; Fig. 2B). Also, the truncated Ufipa Fault segment aligns with the Ufipa Terrane

376   basement fabrics (distributed fabrics). The North Ufipa Fault and Chisi Fault link at a very high

377   angle to form a salient that point basinward (the Chisi Salient).

378   In the central part of the Ufipa Fault (Figs. 6A-C), the fault segments also exhibit

379   curvilinear geometries and the hard linkage of major fault segments occur at high angles

380   (e.g., Kwera relay ramp). The Kwera relay ramp is the largest relay zone along the Ufipa Fault.

381   To the north of the Kwera relay ramp, the fault trends parallel to a magnetic lineament (discrete

382   fabric) that is located to its east, whereas, to the west of this fault segment, the basement is

383   characterized by two cross-cutting sets (NNW-SSE and NW-SE) of distributed fabrics. The

384   NNW-SSE set represent the fabrics of the Ufipa Terrane, but the origin NW-SE is unknown at

385   this time. The Ufipa Fault segments appear to follow the NNW-SSE basement fabrics but side-

386   steps by means of short fault segments that align with the NW-SE fabric set. To the south of the

387   relay ramp, the Ufipa Fault strikes parallel to the Mughese Shear Zone fabric which is colinear

388   with the NNW-SSE set.

389   Towards the southern part of the Ufipa Fault, in Figures 7A-C, we observe that

390   the Ufipa Fault segments exhibit rectilinear geometries such that it is difficult to delineate fault

391   bends that could correspond to breached relay ramps. In addition, we observe a stronger

392   alignment of the Ufipa Fault segments with the Mughese Shear Zone fabric within the area. To

393   the east of the Ufipa Fault, a fault that strikes parallel to the Ufipa Fault separates

394   the Musangano Trough from the Mbozi Block. The Mbozi basement is characterized by

395   metamorphic fabrics that strike WNW-ESE to NW-SE, oblique to the fault but in which subtle

396   bends in the fault trend align with the basement fabric.

397   In the southern part of the Ufipa Fault (Figs. 8A-C), the fault is characterized by two

398   segments. One of the segments represents a rectilinear southward continuation of the Ufipa Fault

399   and is bounded to the east by a linear ridge that separates it from the Musangano Trough (see

400   "Mughese Fault" segment at Tunduma in Figs. 8A-C). The other segment splays away from the

401   former and delineates a curvilinear geometry that looks like those in the northern and central

402   segments of the Ufipa Fault; this curvilinear segment bounds the southernmost part of

403   the Musangano Trough (see "Ufipa Fault" in Figs. 8A-C). Around Kaseye town (see Fig. 8A),

404   the basement is partially buried and more deeply buried around Chitipa to the south. The

405   continuation of the Ufipa Fault is only evident in the aeromagnetic data as a strong magnetic-low

406   lineament that is bounded by bands of magnetic-high lineaments (see magnetic fabrics

407   around Kaseye town in Fig. 8B). Within the Kaseye area, the NW-striking Mughese Shear Zone

408   fabrics are truncated by a discrete N-S trending magnetic-high lineament (see area within purple

409   rectangle in Fig 8C). The magnetic-low lineament that projects as a southward continuation of

410   the Ufipa Fault persists along the Mughese Shear Zone fabric into the Karonga area of the North

411   Basin of Malawi Rift where the Mughese Shear Zone is abruptly truncated by the Karonga Fault

412   (KF in Fig. 8C). The Mbozi Terrane fabric strike NW-SE, at low angles to the trend of the

413   Mughese Shear Zone.

414   Detailed analyses of the onshore faults along the hinge zone of the Northern Malawi Rift

415   (Karonga area) are well documented in Kolawole et al. (2018). Major onshore hinge zone faults

416   include the Karonga Fault (KF), St. Mary Fault (SMF), Kaporo Fault (KPF), Lupaso Fault (LF),

417   Katesula Fault (KTF) and the Mbiri Fault (Figs. 9A-C). Although the Karonga Fault cuts the

418 basement fabric, several basement-rooted buried fault segments along the rift margin align with

419 the fabric of the Mughese Shear Zone (Kolawole et al., 2018). It is interesting to note that

420 the Mbiri Fault, the longest fault (and potentially has the largest throw?) along the rift margin is

421 sub-parallel to the strike of the continuation of the Ufipa Fault into the area ("Mughese Fault" in

422 Fig. 9C). Although segments of the Mbiri Fault appear to align with the Mughese Shear

423 Zone fabic, it is not clear if the fault reactivated the southwestern boundary of the shear zone or

424 if the fault partially aligns with the fabric of the shear zone. However, we observe that for the

425 most part, the side-steps along the Mbiri Fault align with the basement fabric.

426

427 *4.3.2. Northeastern boundary of the RNMRS*

428 In the northern part of the Lupa Fault, the fault trend defines long, rectilinear segments (Fig.

429 10A) and aligns with the Katuma Terrane, similar to those observed in the southern part of

430 the Ufipa Fault where faults align with the trend of the Ufipa Terrane (Fig. 7). Although, the E-

431 W trending fabric of the Usagaran Orogenic Belt dominates the aeromagnetic data along the

432 northeastern Rukwa Rift shoulder (Fig. 10B), we also observe that closer to the Lupa Fault scarp,

433 there are some lineaments that align with the fault. To the southwest of the Lupa Fault (within

434 the rift valley), a strong magnetic-high lineament which correspond to the Chisi Shear Zone (see

435 onshore continuation and outcrop of the shear zone in Fig. 5), strike sub-parallel to the trend of

436 the Lupa Fault, but deviates more significantly southwards (Figs. 4B and 10).

437   The southern part of the Lupa Fault (between the Katuma Terrane and the Rungwe

438 Volcanic Province) is characterized by curvilinear fault segments (Fig. 10 and 11). The Lupa

439 Terrane fabrics are oriented WNW-ESE, oblique to the Lupa Fault trend (Figs. 11A-C).

440 However, subtle steps along the curvilinear fault segments align with the Lupa Terrane fabrics.

441   In the Rungwe Volcanic Province (RVP), the magnetic lineaments strike NW-SE (Fig.

442   11B), similar to those of the Mbozi Terrane (8B and C), and are truncated to the west by a strong

443   NNW-striking magnetic high lineament (white arrows in Fig. 11B). Furthermore, we observe

444   that the volcanic centers align with NNW-striking magnetic gradient superimposed on the NW-

445   striking fabrics (black arrows in Fig. 11B). South of the Rungwe Volcanic Province, segments of

446   the Livingstone Fault system describe rectilinear geometries and align with strong magnetic-high

447   lineaments (shear zone?) in the Upangwa Terrane.

448

449   **5.0 DISCUSSION**

450   *5.1. Rift architecture*

451   The present morphology of the RNMRS reflects the result of multiple episodes of rifting that

452   have affected this part of eastern Africa i.e. a Permo-Triassic rifting episode (Karoo), a

453   Cretaceous episode and the ongoing Cenozoic rifting episode (e.g., Castaing, 1991; Morley et al.,

454   1992). The Rukwa Rift has been described as both a graben (e.g., Zhao et al., 1997) and half-

455   graben (e.g., Kilembe and Rosendahl, 1992) bounded by the oppositely-dipping Ufipa and Lupa

456   normal faults. The Lupa Fault is commonly regarded as the major border fault of the Rukwa Rift

457   due to its larger throw of ~7 km (Peirce and Lipkov, 1988) relative to the Ufipa Fault (Fig. 12);

458   however, it has also been shown that the Cretaceous and Cenozoic sediments in the rift thicken

459   towards both faults (Fig. 12; Morley et al., 1992; Zhao et al., 1997). In this study, our

460   topographical assessments (Fig. 3, profiles 1-7) show that the scarp height of the Ufipa Fault

461   consistently exceeds that of the Lupa Fault through-out the rift segment, thus suggesting

462   significant footwall uplift along the Ufipa Fault.

463   The significantly lower scarp-height of the Lupa Fault suggests either that it has not been

464   very active in Cenozoic times or that it has been heavily eroded since the cessation of Mesozoic

465   rifting. However, based on these observations, we interpret that in the earlier rifting episodes

466   (especially in the Permo-Triassic Karoo episode), the Lupa Fault played the role of the major

467   border fault such that the basin defines a typical half-graben geometry; but in the present

468   Cenozoic phase of rifting, the Ufipa Fault appear to have been preferentially accommodating

469   more strain. Therefore, we suggest that the Rukwa Rift is possibly transitioning into an

470   asymmetric-graben geometry. An asymmetric-graben is a graben with EMVD greater on one

471   border fault compared to the other one, such that the basin polarity has shifted to the fault with

472   the greater 'exposed minimum vertical displacement' (EMVD) (Lao-Davila et al., 2015). The

473   implications of the present Rukwa Rift morphology on the Lupa Fault may reflect temporal and

474   spatial migration of strain accommodation from a previously dominant border fault into another

475   one that has been previously less-dominant. This could possibly be explained by the Scholz and

476   Contreras (1998) suggestion that when a rift-bounding fault attains some limiting offset, motion

477   on the fault will cease, and strain will be transferred to a new fault.

478

479   *5.2. The Southwestern Boundary of the RNMRS and relationships with Precambrian Basement*

480   *Fabric*

481   In the Chisi area, the Northern Ufipa Fault segment terminates against the Chisi Shear Zone

482   along which the Chisi Fault segment developed. The termination of the Ufipa Fault at its

483   intersection with this shear zone exemplifies one of the roles of pre-existing basement structures

484   as temporal and/or spatial mechanical 'barriers' that arrest and delimit the continuous lateral

485   propagation of a fault. Several studies on fracture propagation have demonstrated that fractures

486   are principally bifurcated, blunted, and/or arrested when they intersect discontinuities, stress

487   barriers and/or rock layers of significantly-contrasting mechanical properties along their path of

488   propagation (e.g., Helgeson and Aydin, 1991; Gudmundsson and Brenner, 2001; Zhang et al.,

489   2007; Zhang and Jeffrey, 2008). Other examples of normal fault termination at long-lived

490   basement shear zones include the case of the Albertine-Rhino Graben terminating at the Aswa

491   Shear Zone (Katumwehe et al., 2015) and the Okavango Rift border faults against the Sekaka

492   Shear Zone (Modisi et al., 2000). We suggest that both the reactivation of the Chisi Shear Zone

493   into the Chisi Fault and termination of fault segments at the shear zone demonstrate the strong

494   influence of the Chisi Shear Zone on the development of this part of the Rukwa Rift.

495   Although the northern segments of the Ufipa Fault align with the basement fabrics (Fig.

496   5B-C) and the southern segments show even stronger alignment with the NNW-SSE fabrics of

497   the Ufipa Terrane and/or Mughese Shear Zone (Fig. 7), we find that the central segments of the

498   fault show only partial alignment with this basement fabric (Fig. 6A-C). These observations

499   imply that, although the Ufipa Fault is thought to have largely propagated along the Mughese

500   Shear Zone (Fig. 2; Delvaux et al., 2012), there is stronger control of the Mughese Shear Zone

501   and Ufipa Terrane fabrics on the fault development along its northern and southern segments

502   than in the central part. We suggest that the partial control of these NNW-SSE fabrics on the

503   central Ufipa Fault segments is due to the occurrence of a NW-SE basement fabric set on the

504   Mughese Shear Zone and Ufipa Terrane fabric (Fig. 6). This may also explain the localization of

505   the largest relay zone along the Ufipa Fault at its central segment.

506   The Tunduma-Kaseye area of Malawi, through the Misuku Mountains (Fig. 8A)

507   constitute the southern boundary of the Mbozi Block. Although, the SRTM DEM shows that the

508   sub-aerial expression of the Ufipa Fault dies out roughly mid-way between Tunduma and

509   Kaseye, the filtered aeromagnetic data reveals that in the subsurface, the fault continues across

510   the Kaseye-Chitipa area as a distinct magnetic-low lineament that bounds the Mughese Shear

511   Zone to the south and runs southeastwards into the Karonga area (Fig. 8B). Upon closer

512   observation of the continuation of this strong magnetic-low lineament in the Kaseye-Chitipa

513   area, we find that it cuts-across and offsets a N-S striking magnetic-high lineament which

514   extends 80 km southwards into the Permo-Triassic Luangwa Rift in Zambia. We interpret this N-

515   S lineament as a mafic dike that is possibly related to one of the earlier (Triassic or Cretaceous)

516   episodes of rifting which are known to have been associated with extensive late-stage diking

517   events in the Luangwa Rift (e.g., Van de Velde and De Waele, 1998) and Shire Graben in

518   southern Malawi (Castaing, 1991). Sedimentary deposits in the Kaseye-Chitipa area resulted in

519   the burial and lack of sub-aerial exposure of this structure, thus making this study the first

520   revelation of its existence in Northwestern Malawi.

521   Our analyses of the geometry of the interpreted dike structure (Fig. 13A), here in referred

522   to as the Chitipa Dike, shows a distinct difference in the geometry of the structure to the north

523   where it is cut by the strong magnetic-low lineament (continuation of the Ufipa Fault) and to the

524   south (farther away from the fault intersection). South of Chitipa (Fig. 13B), we observe that the

525   north-trending dike describes a consistent left-stepping geometry which diminishes across the

526   Chitipa town location and continues with a more rectilinear geometry northwards into the

527   Mughese Shear Zone area. This side-stepping geometry is typical of vertical sheet intrusions and

528   are related to either magma intrusion into pre-existing stepped joint systems (e.g., Baer, 1991) or

529   near-surface stress rotations during magma intrusion (e.g., Fossen, 2010). In this study, the

530   coincidence and strike of the dike-steps along the NW- to NNW- striking basement fabric may in

531 fact suggest the possible influence of pre-existing basement fabric on the stepping geometries of

532 dike intrusions during their emplacement in host metamorphic rocks (Fig. 13B).

533   Further north, where the dike is cut by the continuation of the Ufipa Fault, the filtered

534 aeromagnetic data shows the dike exhibiting consistent right-lateral offsets across NW-SE

535 magnetic gradients (Fig. 13C). This clear distinction in the structural style of the dike south of

536 Chitipa and in the north across the continuation of the Ufipa Fault, suggest that the contrasting

537 structural styles are associated with different geological processes. In a summary, we interpret

538 that along the southern boundary of the Mbozi Block, the continuation of the Ufipa Fault, which

539 itself aligns with the Mughese Shear Zone fabric (Fig. 8B-C), is a right-lateral strike-slip fault

540 that displaced a N-S trending Mesozoic (?) dike intrusion (Fig. 13C). We further interpret that

541 this strike-slip fault reactivated the Precambrian Mughese Shear Zone at some time post-

542 Cretaceous (i.e. related to the present Cenozoic rifting phase), and therefore refer to it as the

543 "Mughese Fault". This interpretation is further supported by the change in the morphological

544 expression of the Ufipa Fault from a typical single-scarp style into a narrow linear valley-ridge

545 style in the Tunduma area in the SRTM DEM (see "linear ridge" in Fig. 8A). The observed

546 linear valley-ridge geomorphology is typical of active strike-slip fault zones (e.g., McCalpin et

547 al., 2009). In addition, previous field studies in the area (Delvaux et al., 2012) observed strike-

548 slip displacement on rock outcrops at Tunduma and Mbozi Quarry ("Q" in Fig. 8A). Using the

549 Chitipa Dike as a strain marker, we observe that the offsets increase northwards across multiple

550 splays of the Mughese Fault and estimate that the displacement is maximum at the major

551 Mughese Fault trace (northernmost extent of the strike-slip fault zone). Since mafic intrusions

552 often produce magnetic anomalies larger than the actual size of the sources, it is practically

553 impossible to estimate the true cumulative strike-slip displacement from the aeromagnetic data.

554   However, based on the lateral dike separation across the fault on our aeromagnetic data, we

555   estimate a minimum of 500 m strike-slip displacement along the Mughese Fault (Fig. 13C). In

556   Figure 14, we present a conceptual model that summarizes our interpretation of the Chitipa Dike

557   geometry and the interaction of the Mughese Fault with the dike.

558   In Tunduma area (Fig. 8A), the presence of discrete breaching of the linear ridge by

559   stream channels suggest that the strike-slip displacement along the Mughese Fault is most-likely

560   a short-lived event that occurred at some time in the past during the development of the RNMRS.

561   The curvilinear fault scarp adjacent to the Mughese Fault at Tunduma shows single-scarp

562   morphology (not linear-ridge morphology) typical of normal faults as seen on the other segments

563   of the Ufipa Fault. Therefore, we interpret this curvilinear fault scarp as a possible old segment

564   of the Ufipa Fault that was 'pirated' by the Mughese strike-slip fault; thus, suggesting a phase in

565   which the Ufipa Fault accommodated strike-slip displacement.

566   Along the southwest margin of the North Malawi Rift (Karonga area), the Mughese Fault

567   diffuses into a zone of wide-spread faulting where the southeast-ward bend of the Mughese

568   Shear Zone controls the development of the normal faults and recent seismicity along the basin

569   hinge margin (Fig. 9A-C) (Kolawole et al., 2018; Dawson et al., 2018). Further south of Karonga

570   town, the NNW-striking Mbiri Fault is the dominant fault structure in terms of its length (and

571   displacement?) along this part of the hinge zone of the North Malawi Rift. We do not observe

572   any direct spatial connectivity between the Mughese Fault and the Mbiri Fault. However, based

573   on the sub-parallel geometry of both faults and the structural dominance of the Mbiri Fault in the

574   area, we suggest that the Mbiri Fault could possibly represent a continuation of the Mughese

575   Fault into the hinge zone of the Malawi Rift North Basin. It is also important to note that the

576   Mbiri Fault is synthetic to the Livingstone border Fault. Following the observations and

577   interpretations above, we suggest that there exists a well-developed continuous connectivity of

578   rift-related structures along the southwestern boundary of the RNMRS, facilitated by the extent

579   of the Mughese Shear Zone and the Ufipa Terrane. Interestingly, the linking of the oppositely-

580   dipping Ufipa and Mbiri Faults by the Mughese strike-slip fault describes a structure that,

581   overall, is similar to that of the Morley et al. (1990) convergent-approaching normal fault

582   system.

583

584   *5.3. The Northeastern Boundary of the RNMRS and relationships with Precambrian Basement*

585   *Fabric*

586   The northern segment of the Lupa Fault exhibits clear alignment with the trend of the Katuma

587   Terrane (Fig. 10) and with a few interpretable magnetic lineaments (likely due to low resolution

588   of the aeromagnetic data). We also note that the Lupa Fault is sub-parallel to the Chisi Shear

589   Zone in this area. Farther south of the Lupa Fault (Kapalala-Kanga area; Figs. 10 A-C), the fault

590   segments occur at a high angle to the Usagaran Belt and Lupa Terrane fabrics, thus indicating an

591   apparent lack of control of pre-existing basement fabric on the propagation of the southern Lupa

592   Fault, except in the coincidence of the fault steps with the trend of the basement fabrics.

593   The southern segment of the Lupa Fault transitions into the Rungwe Volcanic Province

594   (RVP) where surficial cover of volcanic deposits obscures the southward continuation of the

595   Lupa Fault (Fig. 11A). In addition, the presence of mafic volcanic deposits in the RVP (e.g.,

596   Fontijn et al., 2012) makes it difficult to make a reliable interpretation of the magnetic fabric of

597   the underlying Precambrian basement (Fig. 11B). However, we find that a distinct magnetic-high

598   lineament aligns with the Mbaka Fault surface trace (white arrows in Figs. 11A and 11B). Also,

599   the distribution of volcanic centers in the RVP show alignment with both the Mbaka Fault trace

600   and a subtle curvilinear gradient (black arrows in Fig. 11B). Further south, the curvilinear

601   gradient connects with the Livingstone Fault, the northeastern border fault of the North Malawi

602   Rift. This curvilinear gradient coincides with the location and extents of the so-called "Ngozi-

603   Rungwe Line" of Fontijn et al. (2010), described as a buried fault system that served as a conduit

604   for magmatic fluids to migrate to the surface volcanic vents. Therefore, although it is possible

605   that the magnetic anomalies in this area are affected by remanent magnetization from the

606   volcanic deposits, we interpret that this aeromagnetic gradient provides a possible subsurface

607   evidence of the fault system (Ngozi-Rungwe Line) that connects the Lupa Fault and the

608   Livingstone Fault across the RVP. The filtered aeromagnetic data and previous field studies

609   (e.g., Wheeler and Karson, 1989) shows that the Livingstone Fault segments align with and

610   reactivated the fabric of the Upangwa Terrane (Figs. 11B-C). The observations and

611   interpretations above suggest that there exists a well-developed continuous connectivity of rift-

612   related structures along the northeastern boundary of the RNMRS. However, the relationship

613   between the basement fabric and the buried faults beneath the volcanic deposits remains unclear.

614

615   *5.4. Implications for Rift Development*

616   *5.4.1. Rift Coupling*

617   In the Rukwa Rift, the substantial dominance of the Ufipa Fault rift shoulder over that of the

618   Lupa Fault may imply that the Ufipa Fault is the present-day active border fault of the Rukwa

619   Rift. This proposition may be supported by the hypocentral location of the 1994 Mw5.9 Rukwa

620   earthquake and its aftershocks with epicentral location in the northern part of the rift (Fig. 12;

621   Zhao et al., 1997). The nodal planes of the earthquake focal mechanism solution are broadly

622   consistent with the orientation of both the Lupa and Ufipa faults, and relative position of

623 aftershocks to the main shock is well determined (Fig. 12; Zhao et al., 1997). Considering the

624 uncertainty range of the earthquakes, the spatial distribution of the aftershocks relative to the

625 main shock delineates a sub-horizontal fault zone that most fits the subsurface projection of the

626 Ufipa Fault (Fig. 12). In addition, field investigations of the Kwera relay ramp (see Fig. 6 for

627 location) revealed features that indicate recent activity along the Ufipa Fault (Delvaux et al.,

628 2012). Camelbeeck and Iranga (1996) observed several lower crustal seismicity in the Rukwa

629 Rift with most of the events clustering beneath the Songwe Trough and the Rungwe Volcanic

630 Province (southern parts of the rift; Fig. 1B). The locations of the clusters suggest activity along

631 the southern Lupa Fault and Mbeya Range Fault. However, since the scarp height (and throw?)

632 of the Ufipa Fault decreases southwards (Fig. 3), and the throw on the Lupa Fault increases

633 southwards (and rapidly along the Songwe Trough) (Morley et al., 1992), we infer that the

634 present border fault role of the Ufipa Fault excludes the southernmost parts of the Rukwa Rift.

635 It has also been observed that the early stage of continental rifting is typically

636 characterized by the development of along-axis alternating polarity of rift segments, rift border

637 faults, uplifted rift flanks (e.g., Bosworth, 1985; Rosendahl, 1987; Hayward and Ebinger, 1996;

638 Lao-Davila et al., 2015). The zones of polarity changes (transfer/accommodation zones) serve to

639 transfer extensional strain between the rift segments and link the border faults which often have

640 variable structural styles and geometries (e.g., Morley et al., 1990; Wilson, 1999). Within young

641 continental rift settings, interactions between these large border faults lead to the systematic

642 coupling of border faults and rift segments across the transfer zones, and subsequent growth of

643 the rift system (e.g., Corti, 2012). Along the RNMRS, the alternating location of the of rift

644 shoulder uplift (SW in Rukwa Rift and NE in North Malawi Rift), typical of coupled rift

645 segments, suggest that the RNMRS can be considered a coupled rift segment. Further, our study

here shows that there is in fact, continuous structural continuation along the northeastern and southwestern margins of the RNMRS, typical of a coupled rift segment. Although, studies in the EARS and illustrations of its rift segments had always assumed this to be true, we hereby provide evidence supporting it, for the first time. In the West Antarctic rift system, the localization of recent volcanism along transverse structures within an accommodation zone (the Discovery accommodation zone) suggests active structural interactions between the flanking rift segments (Wilson, 1999). Therefore, we further suggest that the focusing of Neogene volcanism (e.g., Fontijn et al., 2010, 2012) along the northeastern boundary faults of the Mbozi accommodation zone (Fig. 15A) may be indicative of the ongoing coupling of the Rukwa and North Malawi Rift's northeastern border faults.

5.4.2. Rift Kinematics

Several studies have suggested that the development of the RNMRS has been dominated by dextral strike-slip kinematics (e.g., Chorowicz, 1989; Daly et al., 1989; Wheeler and Karson, 1994; Kervyn et al., 2006; Mortimer et al., 2007). However, analyses of fault architecture, fault-kinematics, paleostress and present-day earthquake focal mechanism solution in the Rukwa Rift show that the present-architecture of the rift largely developed within a pure extensional setting with extension direction orthogonal to the trend of the RNMRS (Morley, 2010; Delvaux et al., 2012). Furthermore, Delvaux et al. (2012) observed dextral strike-slip faulting along the fault systems bounding the Rukwa Rift, but concluded that the strike-slip event was transitory and was associated with an early Mesozoic transpressional event that resulted in the inversion of Karoo sediments. In this study, we observe the existence of a well-defined strike-slip fault bounding the SW margin of the Mbozi Block that reactivated the Precambrian Mughese Shear Zone. We also

669   observe lack of present-day activity along the strike-slip fault, and that this fault displaced a

670   buried mafic dike with at least 500 m of dextral offset.

671   In the absence of chronological data on the mapped dike, we posit that the dike is most-

672   likely associated with the widespread late-Karoo dike swarms observed in the Luangwa Rift and

673   Shire Graben (southern Malawi) (Castaing, 1991; Van de Velde and De Waele, 1998). We refer

674   to this strike-slip fault as the "Mughese Fault", and the buried dike as the "Chitipa Dike". The

675   Chitipa Dike, presented for the first time in this work, may constitute the most excellent record

676   of strike-slip kinematics along the RNMRS. Although, our results agree with Delvaux et al.

677   (2012) in that the strike-slip faulting along the RNMRS was short-lived, we suggest that future

678   geochronological analyses of this intrusion may provide the most-reliable constraint on the

679   timing of strike-slip faulting event. It is also interesting to note that if the Mughese strike-slip

680   fault is post-Karoo, its development represents a late reactivation of the Mughese Shear Zone in

681   the evolution of the RNMRS. However, late reactivation of rift-oblique basement shear zones is

682   not uncommon in rift basins (e.g., Muirhead and Kattenhorn, 2018).

683   Following the considerations above, we present cartoons of the RNMRS, illustrating the

684   continuous structural connectivity along the northeast and southwest boundaries guided by the

685   basement fabrics (Fig. 15B), and possible subsurface geometries and interactions of the domain-

686   bounding structures (Fig. 15B-E). The inferred dominance of the Ufipa Fault in the northern and

687   central parts of the Rukwa Rift (Fig. 12) suggest possible truncation of the Lupa Fault at depth,

688   such that the load of the basin hanging wall block is being carried by the Ufipa Fault (Fig. 15B).

689   However, seismic data is needed to confirm this interpretation. We illustrate a possible spatial

690   relationship between the RVP magma pathways and the Mbozi Block bounding faults in Figure

691   15C. In Figure 15D-E, we show a generalized basin geometry and flip in border fault polarity

692 from the Malawi Rift North Basin to the Usisya Basin. Overall, we posit that, along the

693 northeastern boundary of the Mbozi Block transfer zone strain is accommodated by magmatism

694 utilizing pre-existing fault systems, whereas, along the southwestern boundary, strain is

695 accommodated by dextral strike-slip faulting.

696

697 *5.5. Control of basement fabrics on normal fault geometries*

698 Overall, along the border faults of the Rukwa Rift, we find that strongly-curvilinear normal fault

699 geometries (in plan-view) occur in three distinct settings. One, in areas where the basement

700 fabrics describe high curvatures (>15°) (e.g., in the Chisi area, northern segment of the Lupa

701 Fault; Fig. 5). Second, in areas of superposition of discordant sets of basement fabrics, in which

702 the overall fault strike is parallel to one of the sets and relay ramp breach-faults follow the other

703 fabric set that is oblique to the overall fault strike (e.g., central segment of Ufipa Fault; Fig. 6).

704 Third, in areas where the faults propagate at high-angle to the strike of the basement fabrics (e.g.,

705 in the Kapalala-Kanga area, southern segment of the Lupa Fault; Fig. 10). In general, along the

706 RNMRS, we find that in areas where the basement fabrics show low curvatures (<10°), the fault

707 segments tend to describe long, rectilinear geometries with narrow or almost unidentifiable

708 breached-relay zones (e.g., Southern Ufipa Fault, Fig. 7; Mughese Fault, Fig. 8; Livingstone

709 Fault, Fig. 11). We suggest that the control of rectilinear (<10° curvature) basement fabrics on

710 the propagation of normal faults may result in the development of rectilinear fault segments with

711 greater likelihood of occurrence of narrow relay ramps and tip-to-tip fault linkage.

712 Curvilinear normal faults have been observed at various scales and at different

713 extensional tectonic settings (Fossen and Rotevatn, 2016). However, the first order curvilinear

714 normal faults are typically characterized by segment boundaries with salients (cusps) that plunge

715 basin-ward e.g., Salt-lake salient and Transverse Mountain salients of the Wasatch Fault in Utah

716 (Fig. 16A), and the Gullfaks salient in the North Sea (Fig. 16B) (Fossen and Rotevatn, 2016).

717 Also, the reported curvilinear faults show characteristic basin-ward concave geometries.

718 However, the South Oquirrh Mountains normal fault zone, although curvilinear (Wu and Bruhn,

719 1994), exhibits striking basin-ward convex geometry in which the cusps point into the footwall

720 of the fault (Fig. 16A). Wu and Bruhn (1994) suggested that convex curvilinear geometry of the

721 South Oquirrh Mountains normal fault zone developed by sequential propagation of the fault into

722 its foot-wall, guided by linkage across smaller en-echelon faults created by the lateral shear

723 components at the tips of the propagating fault. Here, in the Rukwa Rift, we observe both

724 convex- and concave-curvilinear normal fault geometries along the Ufipa and Lupa Faults. The

725 central Ufipa Fault (Fig. 6) and southern Lupa Fault (Kapalala-Mwambani area in Fig. 10A-C)

726 exhibit convex-curvilinear normal fault geometries, whereas the northern Ufipa Fault and the

727 Chisi Fault demonstrate concave-curvilinear fault geometries (linked at the Chisi salient) (Fig.

728 5). Also, we find striking similarities between the concave- and convex-curvilinear fault

729 geometries of the Rukwa Rift (Fig. 16C) with those in the southern Malawi Rift (Fig, 16D), the

730 Jurassic sedimentary sequence of the northern North Sea rift (Gullfaks area) (Fig. 16B), and the

731 Provo-Salt Lake City area (Fig. 16A). As show in Figure 16D, the segments of the Bilila-

732 Mtakataka Fault in southern Malawi Rift present excellent examples of convex-curvilinear

733 normal fault geometries (Jackson and Blekinsop, 1997). Recent studies on the relationships

734 between the basement fabrics and the Bilila-Mtakataka Fault segments (Johnson et al., 2018;

735 Hodge et al., 2018) show that some of the segments appear to align with the distributed basement

736 fabrics, while others cut across the basement fabrics.

737   Based on the observations above, we present conceptual models for the control of

738   various configurations of pre-existing basement fabrics on the development of curvilinear normal

739   fault plan-view geometries (Fig. 17). We show how discrete and distributed basement fabrics and

740   combinations of the two categories of fabrics can influence the plan-view geometry of normal

741   faults. However, there is need to better understand (1) the influence of the basement fabrics on

742   the geometries of curvilinear normal faults in 3-dimensions, (2) the influence of the extension

743   direction on the development of the observed curvilinear normal faults in areas where the

744   basement fabric present mechanical anisotropy.

745   Although, Fossen and Rotevatn (2016) provide evidence of subsidiary short-cut faulting

746   across a salient, suggesting an impending evolution of concave-curvilinear faults into rectilinear

747   faults, it is not yet clear if the model applies to convex-curvilinear normal faults since the two

748   styles of faults are geometrically different. However, the synthetic Bilila-Mtakataka and the

749   Chirobwe-Ncheu Faults (Fig. 16D) in southern Malawi Rift may provide some insight. Since the

750   Chirobwe-Ncheu Fault is older than the Bilila-Mtakataka Fault (Jackson and Blekinsop, 1997),

751   the rectilinear geometry of the Chirobwe-Ncheu Fault suggests that the apices of convex

752   curvilinear segments may likewise eventually get breached to form more-rectilinear fault

753   segments. Conversely, we observe the opposite of this model along the Lupa Fault, where the

754   more-rectilinear northern Lupa Fault has accommodated much less strain compared to its

755   curvilinear southern segment which has the most strain within the Rukwa Rift (Morley et al.,

756   1992). Therefore, we suggest that although the model of temporal progression from a curvilinear

757   to rectilinear fault geometry may apply to some large normal faults, it may not apply to others.

758

759

32

5.6. Rift Bifurcation

760

761   The basin scale splaying of the Rukwa Rift around the Mbozi Block into the Musangano

762   and Songwe Troughs (Fig. 1B) obviously represents a smaller-scale of rift bifurcation when

763   compared to the continental scale bifurcation of rift systems around microplates. Examples of

764   such continental-scale rift bifurcation include the branching of the East African Rift around the

765   Tanzania microplate into the western and eastern branches (Fig. 1A; e.g., Rosendahl, B.R., 1987;

766   Versfelt and Rosendahl, 1989), the Red Sea Rift around the Sinai microplate into the Gulf of

767   Suez Rift and Dead Sea Transform, and the South Atlantic Rift around the Sergipe microplate

768   into the Tucano-Recôncavo Rift and Sergipe-Alagoas Transform (e.g., Szatmari and Milani,

769   1999) (Figs. 18A-C). Based on scale distinction, we therefore refer to the continental rift-system

770   scale bifurcation as first (1st) order rift bifurcation (Figs. 18A-C) and the rift-basin scale

771   bifurcation as second (2nd) order rift bifurcation (Fig. 18D-F). Similar to the Rukwa Rift, 2nd

772   order rift bifurcations are common along the East African Rift System. Examples include the

773   Southern Malawi Rift bifurcation around the Shire Horst, the Shire Graben bifurcation around

774   the Namalambo Horst, and the Albertine Graben bifurcation around the Rwenzori Block (Fig.

775   18B; e.g., Castaing, 1991; Koehn et al., 2008; Lao-Davila et al., 2015; Xue et al., 2017).

776   Regardless of scale, numerical models have showed that inherited structural

777   heterogeneity and lateral strength variations are key controls on rift bifurcation (e.g., Brune and

778   Autin, 2013; Brune et al., 2017). However, it appears that 1st order bifurcations commonly occur

779   at the tip of pre-existing microcratonic blocks along the path of propagation of a continental rift

780   system (e.g., Fig. 18A). Also, 2nd order bifurcations appear to occur at the transfer zones between

781   approaching rift segments, possibly due to a high tendency for the development of interfingering

782   fault blocks in the transfer zones between colinear approaching rift segments (Morley, 1995) and

783 lateral rotation of the trapped blocks in the transfer zones between overlapping approaching rift

784 segments (Koehn et al., 2008).

785   It is possible that the bifurcation of the Rukwa Rift around the Mbozi Block is related to

786 the location of the block within the transfer zone of the colinear approaching Rukwa and North

787 Malawi Rift segments. However, we suggest that the basement fabrics of the Ubendian Belt

788 around the Mbozi Block transfer zone could be playing a complementary role in facilitating and

789 guiding the intra-rift bifurcation of the Rukwa Rift around the block. Our filtered aeromagnetic

790 map (Fig. 4B) shows that the block is dominated by a WNW-ESE and N-S fabrics. According to

791 Daly (1988), the Meta-basites and intermediate granulites and quartzites of the Mbozi Block are

792 characterized by lineations that trend NE-SW. These observations, however, suggest that the

793 Mbozi Block fabrics strike at oblique to high-angles to the trend of the colinear fabrics of the

794 basement terranes bounding the Mbozi Block (Katuma-Upangwa Terranes to the northeast, and

795 those of the Ufipa Terrane to the southwest) and the main rift-bounding faults (the Lupa, Ufipa,

796 Livingstone and Mughese Faults) (Fig. 15A). Therefore, we suggest that the colinear fabrics of

797 the basement terranes surrounding the Mbozi Block which are already controlling the

798 propagation and linking of the rift-bounding faults may be playing a significant role in guiding

799 the bifurcation of the Rukwa Rift around the Mbozi Block (Figs. 4B, 7, 8 and 11).

800

801 **6.0 CONCLUSIONS**

802   Our topographic analyses of the morphology of the RNMRS and detailed study of the

803 relationships between the pre-existing basement fabric and rift-related faults provide, for the first

804 time, evidence supporting the coupling of the Rukwa and North Malawi Rift. Our topographic

805 analyses in the Rukwa Rift suggest that the Ufipa Fault is the present-day active border fault of

806 the rift. We find that the Ufipa fault is the dominant topographic feature in the northern part of

807 the RMNRS and diminishes as it encounters the Mbozi block where it becomes a strike slip fault

808 (Mughese Fault), at which point the border fault polarity flips and the Livingstone Fault is the

809 dominant fault in the southern part of the RNMRS.

810 Further, we demonstrate the continuity structures along the northeastern and

811 southwestern margins of the RNMRS. We show that this structural connectivity across the

812 Mbozi Block transfer zone between the rifts is guided by the pre-existing Precambrian terrane

813 fabrics and associated shear zones. We show that the coupling of the RNMRS along the

814 northeastern boundary of the Mbozi Block transfer zone is accommodated by magmatism along

815 the linking faults, whereas, coupling along the southwestern boundary is accommodated by

816 strike-slip faulting. Overall, we suggest that the continuation of the boundary faults along the

817 RNMRS, and their alignment with colinear Precambrian basement fabric and shear zones

818 indicate the influence of the pre-existing basement structures on the coupling and amalgamation

819 of approaching colinear rift segments. On the basin-scale bifurcation of the Rukwa Rift, we infer

820 that the discordance of the basement fabrics within the Mbozi Block transfer zone to those of the

821 basement terranes bounding it may have facilitated the development of intra-rift bifurcation of

822 the rift around the transfer zone.

823 Furthermore, we show the influence of pre-existing basement fabrics on the development

824 of the RNMRS as evidenced in the geometry, termination and kinematics of the rift-bounding

825 fault segments. Our observations suggest that curvilinear normal fault geometries developed in

826 areas where the basement fabrics are either curvilinear, composed of superposed sets of

827 differently-oriented fabrics, or not favorably oriented to the extensional stress field. Whereas,

828 long, rectilinear fault geometries with narrow or almost unidentifiable breached-relay zones

829   developed in areas where the pre-existing basement fabrics are roughly rectilinear, suggesting

830   the greater likelihood of occurrence of tip-to-tip linkage of fault segments.

831   Finally, we present the existence of a buried Pre-Cenozoic strike-slip-faulted mafic dike,

832   which we suggest is potentially the most excellent record of strike-slip kinematics along the

833   RNMRS. We further suggest that future geochronological analyses of this intrusion may provide

834   the most-reliable constraint on the timing of the controversial strike-slip faulting event along the

835   RNMRS.

836

837   **Acknowledgements**

846

847   **References**

848   Baer, G., 1991. Mechanisms of dike propagation in layered rocks and in massive, porous

849   sedimentary rocks. *Journal of Geophysical Research: Solid Earth*, *96*(B7), pp.11911-

850   11929.

851   Baranov, V., 1957. A new method for interpretation of aeromagnetic maps: pseudo-gravimetric

852   anomalies. *Geophysics*, *22*(2), pp.359-382.

853   Borrego, D.J., 2016. Crustal Structure of the Rungwe Volcanic Province and Region

854   Surrounding the Northern Lake Malawi Rift Basin. MSc Thesis, Pennsylvania State

855   University.

856   Bosworth, W., 1985. Geometry of propagating continental rifts. *Nature*, *316*(6029), p.625.

857   Boven, A., Theunissen, K., Sklyarov, E., Klerkx, J., Melnikov, A., Mruma, A. and Punzalan, L.,

858   1999. Timing of exhumation of a high-pressure mafic granulite terrane of the

859   Paleoproterozoic Ubende belt (West Tanzania). *Precambrian Research, 93*(1), pp.119-

860   137.

861   Brune, S. and Autin, J., 2013. The rift to break-up evolution of the Gulf of Aden: Insights from

862   3D numerical lithospheric-scale modelling. *Tectonophysics, 607*, pp.65-79.

863   Brune, S., Corti, G. and Ranalli, G., 2017. Controls of inherited lithospheric heterogeneity on rift

864   linkage: Numerical and analog models of interaction between the Kenyan and Ethiopian

865   rifts across the Turkana depression. *Tectonics, 36*(9), pp.1767-1786.

866   Camelbeeck, T. and Iranga, M.D., 1996. Deep crustal earthquakes and active faults along the

867   Rukwa trough, eastern Africa. *Geophysical Journal International, 124*(2), pp.612-630.

868   Castaing, C., 1991. Post-Pan-African tectonic evolution of South Malawi in relation to the

869   Karroo and recent East African rift systems. *Tectonophysics, 191*(1-2), pp.55-73.

870   Chorowicz, J., 1989. Transfer and transform fault zones in continental rifts: examples in the

871   Afro-Arabian rift system. Implications of crust breaking. *Journal of African Earth*

872   *Sciences (and the Middle East), 8(2-4)*, pp.203-214.

873   Chorowicz, J., 2005. The east African rift system. *Journal of African Earth Sciences*, *43*(1),

874   pp.379-410.

875   Collanega, L., Bell, R., Coleman, A.J., Lenhart, A. and Breda, A., 2018. How do intra-basement

876   fabrics influence normal fault growth? Insights from the Taranaki Basin, offshore New

877   Zealand. EarthArxiv, DOI: 10.31223/osf.io/8rn9u

878   Corti, G., 2012. Evolution and characteristics of continental rifting: Analog modeling-inspired

879   view and comparison with examples from the East African Rift System. *Tectonophysics,*

880   *522*, pp.1-33.

881   Daly, M.C., 1988. Crustal Shear Zones in Central Africa - A kinematic approach to Proterozoic

882   Tectonics. *Episodes*, *11*(1), pp.5-11.

883   Daly, M.C., Chorowicz, J. and Fairhead, J.D., 1989. Rift basin evolution in Africa: the influence

884   of reactivated steep basement shear zones. *Geological Society, London, Special*

885   *Publications, 44*(1), pp.309-334.

886   Dawson, S.M., Laó-Dávila, D.A., Atekwana, E.A. and Abdelsalam, M.G., 2018. The influence

887   of the Precambrian Mughese Shear Zone structures on strain accommodation in the

888   northern Malawi Rift. *Tectonophysics*, *722*, pp.53-68.

889   Delvaux, D., and Hanon, M., 1991. Neotectonics of the Mbeya area, SW Tanzania. *Annual*

890   *report of the Royal Museum of Central Africa, Department of Geology and*

891   *Mineralogy*, *1992*, pp.87-97.

892   Delvaux, D., Kervyn, F., Macheyeki, A.S. and Temu, E.B., 2012. Geodynamic significance of

893   the TRM segment in the East African Rift (W-Tanzania): Active tectonics and paleostress

894   in the Ufipa plateau and Rukwa basin. *Journal of Structural Geology*, *37*, pp.161-180.

895   Delvaux, D., Levi, K., Kajara, R. and Sarota, J., 1992. Cenozoic paleostress and kinematic

896   evolution of the Rukwa–North Malawi rift valley (East African Rift System). *Bulletin des*

897   *Centres de Recherche Exploration-Production ElfAquitaine*, *16*, pp.383-406.

898   Fernandez-Alonso, M., Delvaux, D., Klerkx, J. and Theunissen, K., 2001. Structural link

899   between Tanganyika-and Rukwa-rift basins at Karema-Nkamba (Tanzania): basement

900   structural control and recent evolution. *Mus. Roy. Afr. Centr., Tervuren (Belgique), Dép.*

901   *Géol. Min., Rap. Ann*, pp.91-100.

902   Fontijn, K., Delvaux, D., Ernst, G.G., Kervyn, M., Mbede, E. and Jacobs, P., 2010. Tectonic

903   control over active volcanism at a range of scales: case of the Rungwe Volcanic

904   Province, SW Tanzania; and hazard implications. *Journal of African Earth Sciences,*

905   *58*(5), pp.764-777.

906   Fontijn, K., Williamson, D., Mbede, E. and Ernst, G.G., 2012. The Rungwe Volcanic Province,

907   Tanzania–A volcanological review. *Journal of African Earth Sciences*, *63*, pp.12-31.

908   Fossen, H., 2010. *Structural geology*. Cambridge University Press.

909   Fossen, H. and Rotevatn, A., 2016. Fault linkage and relay structures in extensional settings—A

910   review. *Earth-Science Reviews, 154*, pp.14-28.

911   Foster, A., Ebinger, C., Mbede, E. and Rex, D., 1997. Tectonic development of the northern

912   Tanzanian sector of the East African Rift System. *Journal of the Geological*

913   *Society*, *154*(4), pp.689-700.

914   Fritz, H., Abdelsalam, M., Ali, K.A., Bingen, B., Collins, A.S., Fowler, A.R., Ghebreab, W.,

915   Hauzenberger, C.A., Johnson, P.R., Kusky, T.M. and Macey, P., 2013. Orogen styles in

916   the East African Orogen: a review of the Neoproterozoic to Cambrian tectonic

917   evolution. *Journal of African Earth Sciences*, *86*, pp.65-106.

918   Gawthorpe, R.L., Jackson, C.A.L., Young, M.J., Sharp, I.R., Moustafa, A.R. and Leppard, C.W.,

919   2003. Normal fault growth, displacement localisation and the evolution of normal fault

920   populations: the Hammam Faraun fault block, Suez rift, Egypt. *Journal of Structural*

921   *Geology, 25*(6), 883-895.

922   Grauch, V.J.S. and Hudson, M.R., 2007. Guides to understanding the aeromagnetic expression of

923   faults in sedimentary basins: Lessons learned from the central Rio Grande rift, New

924   Mexico. *Geosphere*, *3*(6), pp.596-623.

925   Grauch, V.J.S. and Hudson, M.R., 2011. Aeromagnetic anomalies over faulted strata. *The*

926   *Leading Edge*, *30*(11), pp.1242-1252.

927   Gudmundsson, A. and Brenner, S.L., 2001. How hydrofractures become arrested. *Terra*

928   *Nova*, *13*(6), pp.456-462.

929   Hayward, N.J. and Ebinger, C.J., 1996. Variations in the along-axis segmentation of the Afar

930   Rift system. *Tectonics*, *15*(2), pp.244-257.

931   Helgeson, D.E. and Aydin, A., 1991. Characteristics of joint propagation across layer interfaces

932   in sedimentary rocks. *Journal of Structural Geology*, *13*(8), pp.897-911.

933   Henderson, R.G. and Zietz, I., 1949. The upward continuation of anomalies in total magnetic

934   intensity fields. *Geophysics*, *14*(4), pp. 517-534.

935 Hodge, M., Fagereng, Å., Biggs, J., and Mdala, H., 2018.. Controls on early-rift geometry: New

936   perspectives from the Bilila-Mtakataka fault, Malawi. *Geophysical Research Letters, 45*,

937   3896–3905.

938 Hodgson, I., Illsley-Kemp, F., Gallacher, R.J., Keir, D., Ebinger, C.J. and Mtelela, K., 2017.

939   Crustal structure at a young continental rift: A receiver function study from the

940   Tanganyika Rift. *Tectonics*, *36*(12), pp.2806-2822.

941 Jackson, J. and Blenkinsop, T., 1997. The Bilila-Mtakataka fault in Malaŵi: An active, 100-km

942   long, normal fault segment in thick seismogenic crust. *Tectonics*, *16*(1), pp.137-150.

943 Johnson, S., Mendez, K., Beresh, S.C.M., Mynatt, W.G., Elifritz, E.A., Laó-Dávila, D.A.,

944   Atekwana, E.A., Abdelsalam, M.G., Chindandali, P.R.N., Chisenga, C. and Gondwe, S.,

945   2017.. The Relationships of Subparallel Synthetic Faults and Pre-existing Structures in

946   the Central Malawi Rift. *AGU Fall Meeting poster number T22C-03*.

947 Katumwehe, A.B., Abdelsalam, M.G. and Atekwana, E.A., 2015. The role of pre-existing

948   Precambrian structures in rift evolution: The Albertine and Rhino grabens,

949   Uganda. *Tectonophysics*, *646*, pp.117-129.

950 Kervyn, F., Ayub, S., Kajara, R., Kanza, E. and Temu, B., 2006. Evidence of recent faulting in

951   the Rukwa rift (West Tanzania) based on radar interferometric DEMs. *Journal of African*

952   *Earth Sciences*, *44*(2), pp.151-168.

953 Kilembe, E.A. and Rosendahl, B.R., 1992. Structure and stratigraphy of the Rukwa

954   rift. *Tectonophysics*, *209*(1-4), pp.143-158.

955 Kim, S., Nyblade, A.A. and Baag, C.E., 2009. Crustal velocity structure of the Rukwa Rift in the

956   western branch of the East African Rift system. *South African Journal of Geology*, *112*(3-

957   4), pp.251-260.

958   Kinabo, B.D., Atekwana, E.A., Hogan, J.P., Modisi, M.P., Wheaton, D.D. and Kampunzu, A.B.,

959   2007. Early structural development of the Okavango rift zone, NW Botswana. *Journal of*

960   *African Earth Sciences*, *48*(2), pp.125-136.

961   Kinabo, B.D., Hogan, J.P., Atekwana, E.A., Abdelsalam, M.G. and Modisi, M.P., 2008. Fault

962   growth and propagation during incipient continental rifting: Insights from a combined

963   aeromagnetic and Shuttle Radar Topography Mission digital elevation model

964   investigation of the Okavango Rift Zone, northwest Botswana. *Tectonics*, *27*(3).

965   Koehn, D., Aanyu, K., Haines, S. and Sachau, T., 2008. Rift nucleation, rift propagation and the

966   creation of basement micro-plates within active rifts. *Tectonophysics, 458*(1-4), pp.105-

967   116.

968   Kolawole, F., Atekwana, E.A., Laó-Dávila, D.A., Abdelsalam, M.G., Chindandali, P.R., Salima,

969   J. and Kalindekafe, L., 2018. Active deformation of Malawi Rift's North Basin hinge

970   zone modulated by reactivation of pre-existing Precambrian shear zone fabric. *Tectonics,*

971   *37*, pp.683–704.

972   Lao-Davila, D.A., Al-Salmi, H.S., Abdelsalam, M.G. and Atekwana, E.A., 2015. Hierarchical

973   segmentation of the Malawi Rift: The influence of inherited lithospheric heterogeneity

974   and kinematics in the evolution of continental rifts. *Tectonics*, *34*(12), pp.2399-2417.

975   Lawley, C.J., Selby, D., Condon, D.J., Horstwood, M., Millar, I., Crowley, Q. and Imber, J.,

976   2013. Lithogeochemistry, geochronology and geodynamic setting of the Lupa Terrane,

977   Tanzania: implications for the extent of the Archean Tanzanian Craton. *Precambrian*

978   *Research, 231*, pp.174-193.

979 Lenoir, J.L., Liégeois, J.P., Theunissen, K. and Klerkx, J., 1994. The Palaeoproterozoic

980   Ubendian shear belt in Tanzania: geochronology and structure. *Journal of African Earth*

981   *Sciences*, *19*(3), pp.169-184.

982 Mbede, E.I., 2002. Interpretation of refelction seismic data from the Usangu Basin, East African

983   Rift System. *Tanzania Journal of Science, 28*(1), pp.83-97.

984 McCalpin, J.P., Rockwell, T.K. and Weldon II, R.J., 2009. Paleoseismology of Strike-Slip

985   Tectonic Environments. *International Geophysics, 95*, pp.421-496.

986 Modisi, M.P., Atekwana, E.A., Kampunzu, A.B. and Ngwisanyi, T.H., 2000. Rift kinematics

987   during the incipient stages of continental extension: Evidence from the nascent Okavango

988   rift basin, northwest Botswana. *Geology, 28*(10), pp.939-942.

989 Morley, C.K., 1995. Developments in the structural geology of rifts over the last decade and their

990   impact on hydrocarbon exploration. *Geological Society, London, Special*

991   *Publications*, *80*(1), pp.1-32.

992 Morley, C.K., 2010. Stress re-orientation along zones of weak fabrics in rifts: An explanation

993   for pure extension in 'oblique' rift segments?. *Earth and Planetary Science*

994   *Letters*, *297*(3), pp.667-673.

995 Morley, C.K., Cunningham, S.M., Harper, R.M. and Wescott, W.A., 1992. Geology and

996   geophysics of the Rukwa rift, East Africa. *Tectonics, 11*(1), pp.69-81.

997 Morley, C.K., Nelson, R.A., Patton, T.L. and Munn, S.G., 1990. Transfer zones in the East

998   African rift system and their relevance to hydrocarbon exploration in rifts (1). *AAPG*

999   *Bulletin, 74*(8), pp.1234-1253.

1000   Mortimer, E., Paton, D.A., Scholz, C.A., Strecker, M.R. and Blisniuk, P., 2007. Orthogonal to

1001   oblique rifting: effect of rift basin orientation in the evolution of the North basin, Malawi

1002   Rift, East Africa. *Basin Research*, *19*(3), pp.393-407.

1003   Muirhead, J.D. and Kattenhorn, S.A., 2018. Activation of preexisting transverse structures in an

1004   evolving magmatic rift in East Africa. *Journal of Structural Geology, 106*, pp.1-18.

1005   Njinju, E.A., Atekwana, E.A., Stamps, D.S., Abdelsalam, M.G., Atekwana, E.A., Mickus, K.L.,

1006   Kolawole, F. and Nyalugwe, V., 2018. Lithospheric Structure of the Malawi Rift:

1007   Implications for Rifting Processes in Magma Poor Rift Systems. *EarthArXiv*, DOI:

1008   10.31223/osf.io/83qd9

1009   Peirce, J.W. and Lipkov, L., 1988. Structural interpretation of the Rukwa rift, Tanzania.

1010   *Geophysics, 53*(6), pp.824-836.

1011   Phillips, T.B., Jackson, C.A., Bell, R.E., Duffy, O.B. and Fossen, H., 2016. Reactivation of

1012   intrabasement structures during rifting: A case study from offshore southern

1013   Norway. *Journal of Structural Geology*, *91*, pp.54-73.

1014   Pik, R., Marty, B., Carignan, J., Yirgu, G. and Ayalew, T., 2008. Timing of East African Rift

1015   development in southern Ethiopia: Implication for mantle plume activity and evolution of

1016   topography. *Geology, 36*(2), pp.167-170.

1017   Ring, U., Kröner, A., Buchwaldt, R., Toulkeridis, T. and Layer, P.W., 2002. Shear-zone patterns

1018   and eclogite-facies metamorphism in the Mozambique belt of northern Malawi, east-

1019   central Africa: implications for the assembly of Gondwana. *Precambrian*

1020   *Research*, *116*(1), pp.19-56.

1021   Rosendahl, B.R., 1987. Architecture of continental rifts with special reference to East

1022   Africa. *Annual Review of Earth and Planetary Sciences*, *15*(1), pp.445-503.

1023   Rotevatn, A., Jackson, C.A.L., Tvedt, A.B.M., Bell, R. and Blækkan, I., 2018. How do normal

1024   faults grow?. EarthArXiv.

1025   Salem, A., Williams, S., Fairhead, J.D., Ravat, D. and Smith, R., 2007. Tilt-depth method: A

1026   simple depth estimation method using first-order magnetic derivatives. *The Leading*

1027   *Edge*, *26*(12), pp.1502-1505.

1028   Sarafian, E., Evans, R.L., Abdelsalam, M.G., Atekwana, E., Elsenbeck, J., Jones, A.G. and

1029   Chikambwe, E., 2018. Imaging Precambrian lithospheric structure in Zambia using

1030   electromagnetic methods. *Gondwana Research*, *54*, pp.38-49.

1031   Schenk, V., Boniface, N., Loose, D., Alkmim, F.F. and Noce, C.M., 2006. Paleoproterozoic

1032   subduction zones at the margins of the Tanzania and Congo Cratons: evidence from

1033   eclogites with MORB-type chemistry in the Usagaran–Ubendian Belts of Tanzania and

1034   the Nyong complex of Cameroon. *The Paleoproterozoic Record of the São Francisco*

1035   *Craton*, pp.102-103.

1036   Scholz, C.H. and Contreras, J.C., 1998. Mechanics of continental rift

1037   architecture. *Geology*, *26*(11), pp.967-970.

1038   Silva, J.B., 1986. Reduction to the pole as an inverse problem and its application to low-latitude

1039   anomalies. *Geophysics*, *51*(2), pp.369-382.

1040   Siuda, K., Magee, C., Bell, R., Jackson, C.A.L. and Collanega, L., 2018. Pre-existing basement

1041   thrusts influence rifting in the Taranaki Basin, New Zealand. EarthArXiv.

1042   Szatmari, P. and Milani, E.J., 1999. Microplate rotation in northeast Brazil during South Atlantic

1043   rifting: Analogies with the Sinai microplate. *Geology, 27*(12), pp.1115-1118.

1044 Taylor, B., Weiss, J.R., Goodliffe, A.M., Sachpazi, M., Laigle, M. and Hirn, A., 2011. The

1045   structures, stratigraphy and evolution of the Gulf of Corinth rift, Greece. *Geophysical*

1046   *Journal International, 185*(3), pp.1189-1219.

1047 Theunissen, K., Klerkx, J., Melnikov, A. and Mruma, A., 1996. Mechanisms of inheritance of

1048   rift faulting in the western branch of the East African Rift, Tanzania. *Tectonics, 15*(4),

1049   pp.776-790.

1050 Van de Velde, P., and De Waele, B., 1998. Geology of the Mupamadzi River area. Explanation

1051   of degree sheet 1231, SW quarter, Report No. 105, *Geological Survey Department,*

1052   *Republic of Zambia.*

1053 Versfelt, J. and Rosendahl, B.R., 1989. Relationships between pre-rift structure and rift

1054   architecture in Lakes Tanganyika and Malawi, East Africa. *Nature, 337*(6205), p.354.

1055 Wheeler, W.H. and Karson, J.A., 1989. Structure and kinematics of the Livingstone Mountains

1056   border fault zone, Nyasa (Malawi) Rift, southwestern Tanzania. *Journal of African Earth*

1057   *Sciences (and the Middle East)*, *8*(2-4), pp.393-413.

1058 Wheeler, W.H. and Karson, J.A., 1994. Extension and subsidence adjacent to a "weak"

1059   continental transform: An example from the Rukwa rift, East Africa. *Geology*, *22*(7),

1060   pp.625-628.

1061 Wichura, H., Bousquet, R., Oberhänsli, R., Strecker, M.R. and Trauth, M.H., 2011. The Mid-

1062   Miocene East African Plateau: a pre-rift topographic model inferred from the

1063   emplacement of the phonolitic Yatta lava flow, Kenya. *Geological Society, London,*

1064   *Special Publications, 357*(1), pp.285-300.

1065 Wilson, T.J., 1999. Cenozoic structural segmentation of the Transantarctic Mountains rift flank

1066   in southern Victoria Land. *Global and Planetary Change*, *23*(1-4), pp.105-127.

1067 Wu, D. and Bruhn, R.L., 1994. Geometry and kinematics of active normal faults, South Oquirrh

1068   Mountains, Utah: implication for fault growth. *Journal of Structural Geology*, *16*(8),

1069   pp.1061-1075.

1070   Xue, L., Gani, N.D. and Abdelsalam, M.G., 2017. Geomorphologic proxies for bedrock rivers:

1071   A case study from the Rwenzori Mountains, East African Rift system. *Geomorphology,*

1072   *285*, pp.374-398.

1073 Zhang, X. and Jeffrey, R.G., 2008. Reinitiation or termination of fluid-driven fractures at

1074   frictional bedding interfaces. *Journal of Geophysical Research: Solid Earth, 113*(B8).

1075 Zhang, X., Jeffrey, R.G. and Thiercelin, M., 2007. Deflection and propagation of fluid-driven

1076   fractures at frictional bedding interfaces: a numerical investigation. *Journal of Structural*

1077   *Geology*, *29*(3), pp.396-410.

1078 Zhao, M., Langston, C.A., Nyblade, A.A. and Owens, T.J., 1997. Lower-crustal rifting in the

1079   Rukwa graben, East Africa. *Geophysical Journal International, 129*(2), pp.412-420.

1080

1081

1082

1083

1084

1085

1086

1087

1088

1089

1090

1091

1092

1093

1094

1095

1096

1097

1098

1099

1100

1101

1102
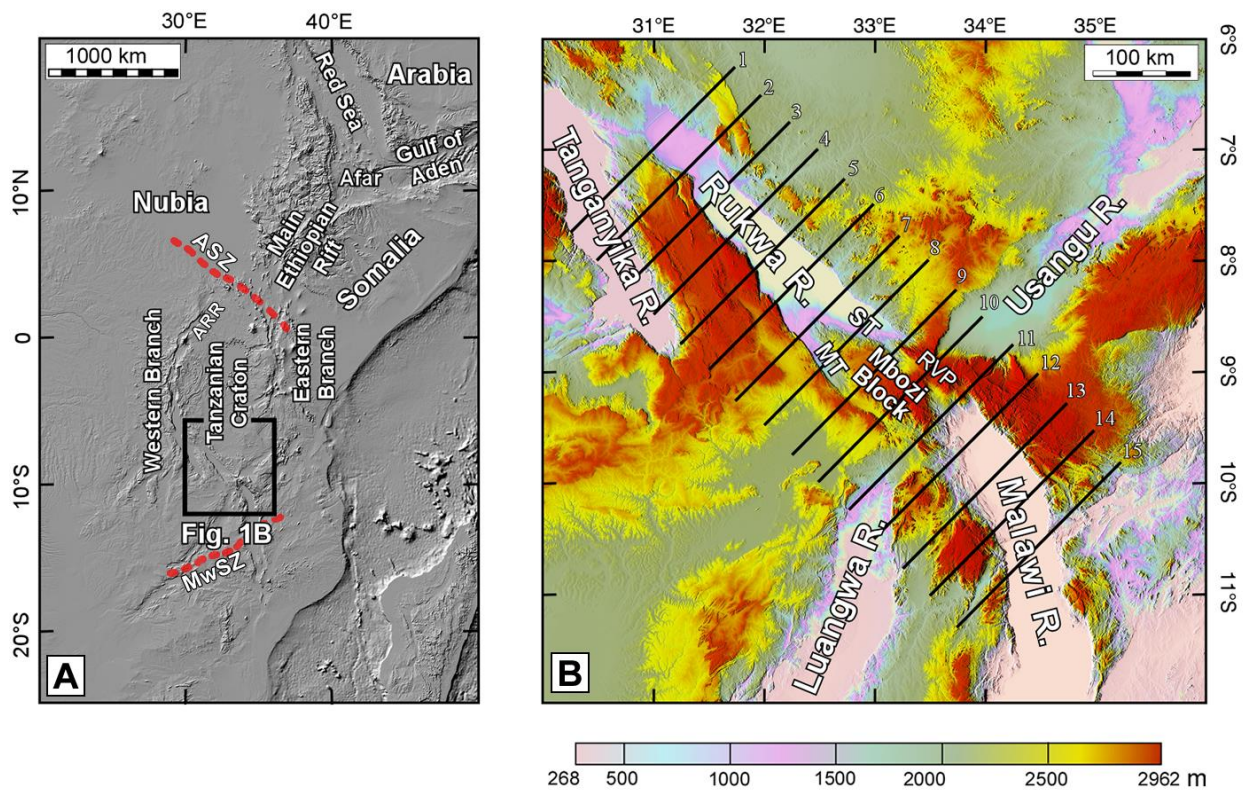
1103

Fig.1. (A) Topographic map of the East African Rift System, showing the segments of the rift system and the location of the Rukwa-North Malawi Rift Segment (RNMRS) (black square). (B) Digital Elevation Model (DEM) of the RNMRS showing the different domains. Solid black lines represent topographic profile lines shown in Figure 3. ARR= Albertine-Rhino Rift, ASZ= Aswa

Shear Zone, MT= Musangano Trough, MwSZ= Mwembeshi Shear Zone, RVP= Rungwe
Volcanic Province, ST= Songwe Trough.
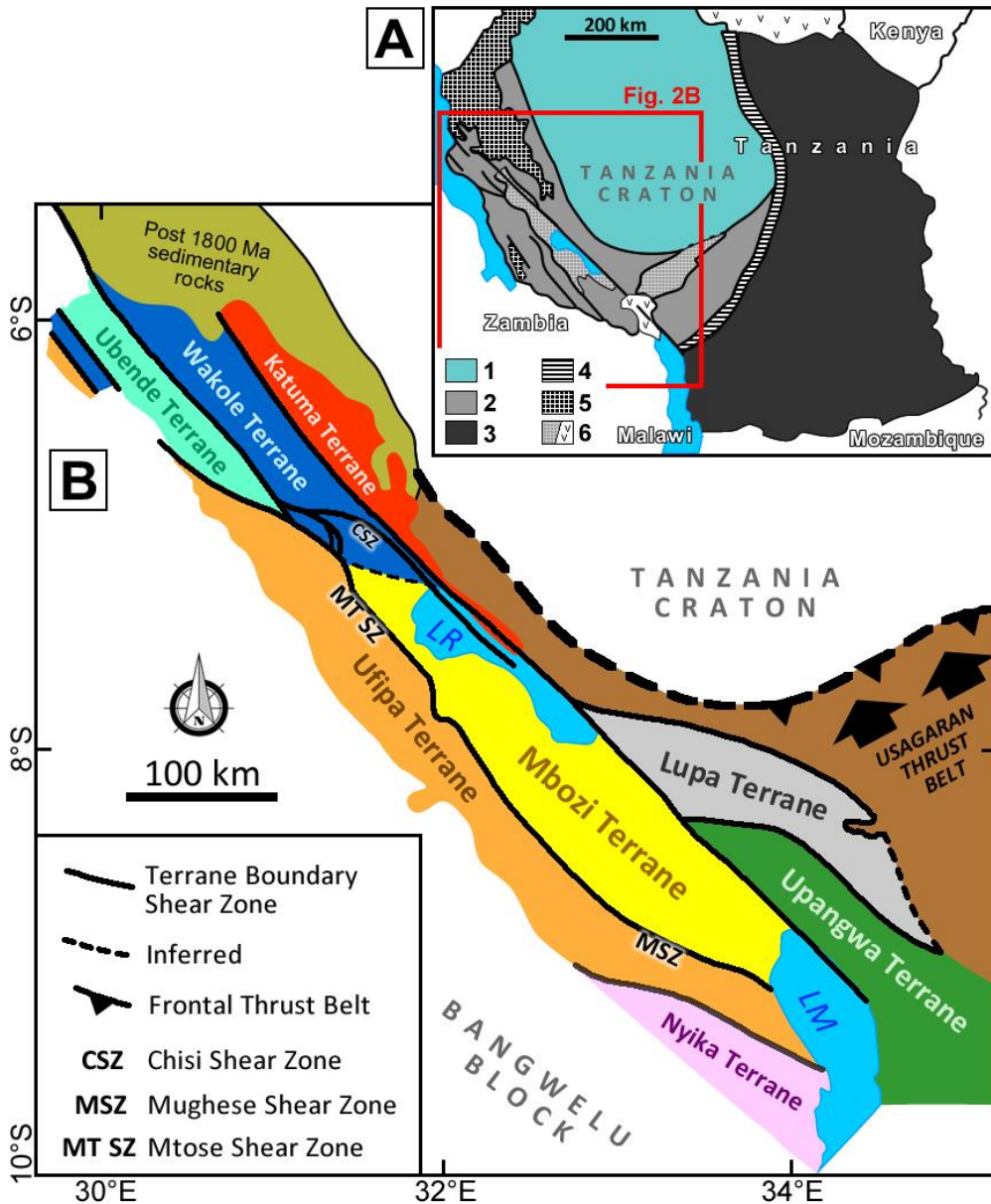
Fig. 2. (A) Precambrian domains around the Tanzanian Craton (modified after Theunissen et al.,
1996; Boven et al., 1999; Fernandez-Alonso et al., 2001; Schenk et al., 2006). 1 = Archean
craton; 2 = Paleoproterozoic Usagaran and Ubendian orogenic belts; 3 = Mozambique orogenic
belt; 4 = western limit of Pan-African influence; 5 = Meso and/or Neoproterozoic sediments
(only for the Ubendian Belt region); 6 = Phanerozoic volcanics and sedimentary rocks. (B)
Regional geological map of southwest Tanzania showing the terrane structure of the Ubendian
orogenic belt within which the Rukwa-Malawi Rift Segment (RNMRS) developed.

49

1139

1140

1141
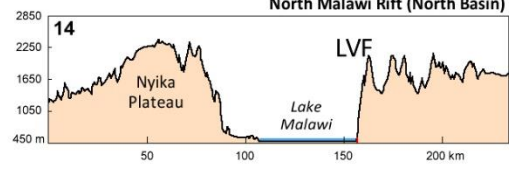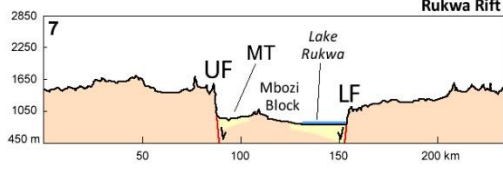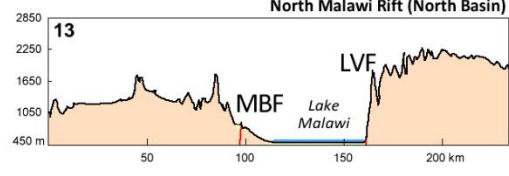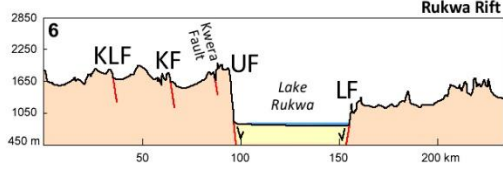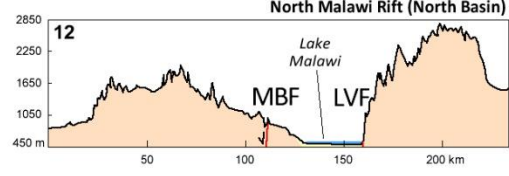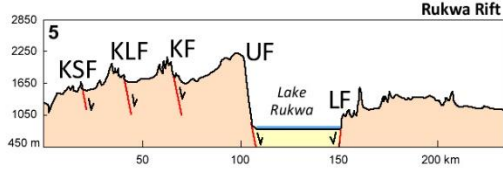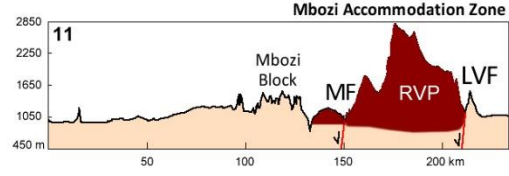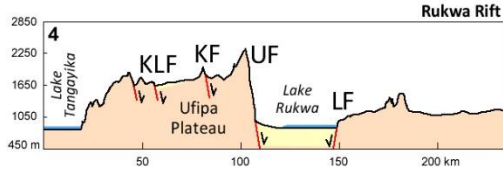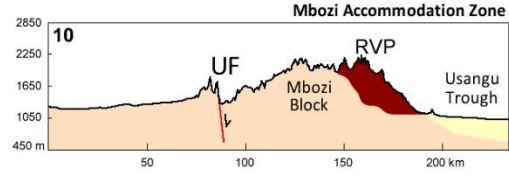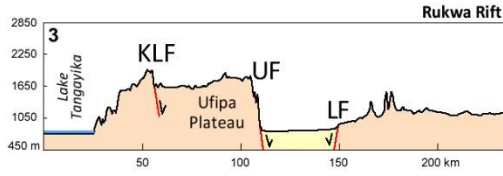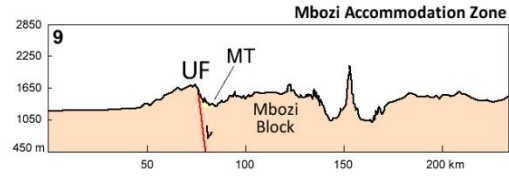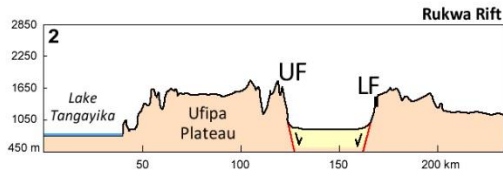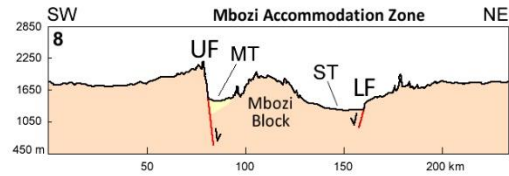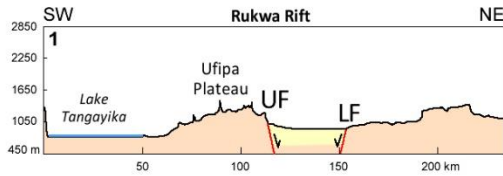
Legend:
- Normal Fault
- Cenozoic Sediments
- Rungwe Volcanics
- Precambrian Basement

50

Fig. 3. Topographic profiles across the Rukwa - North Malawi Rift segment. Profile numbers correspond to the profiles in Figure 1B. KLF = Kalambo Fault, KF = Kanda Fault, KSF = Kasanga Fault, LF = Lupa Fault, LVF = Livingstone Fault, MB = Mbozi Block, MBF = Mbiri Fault, MF = Mbaka Fault, MT = Musangano Trough, RVP = Rungwe Volcanic Province, ST = Songwe Trough, UF = Ufipa Fault, USF = Usisya Fault.
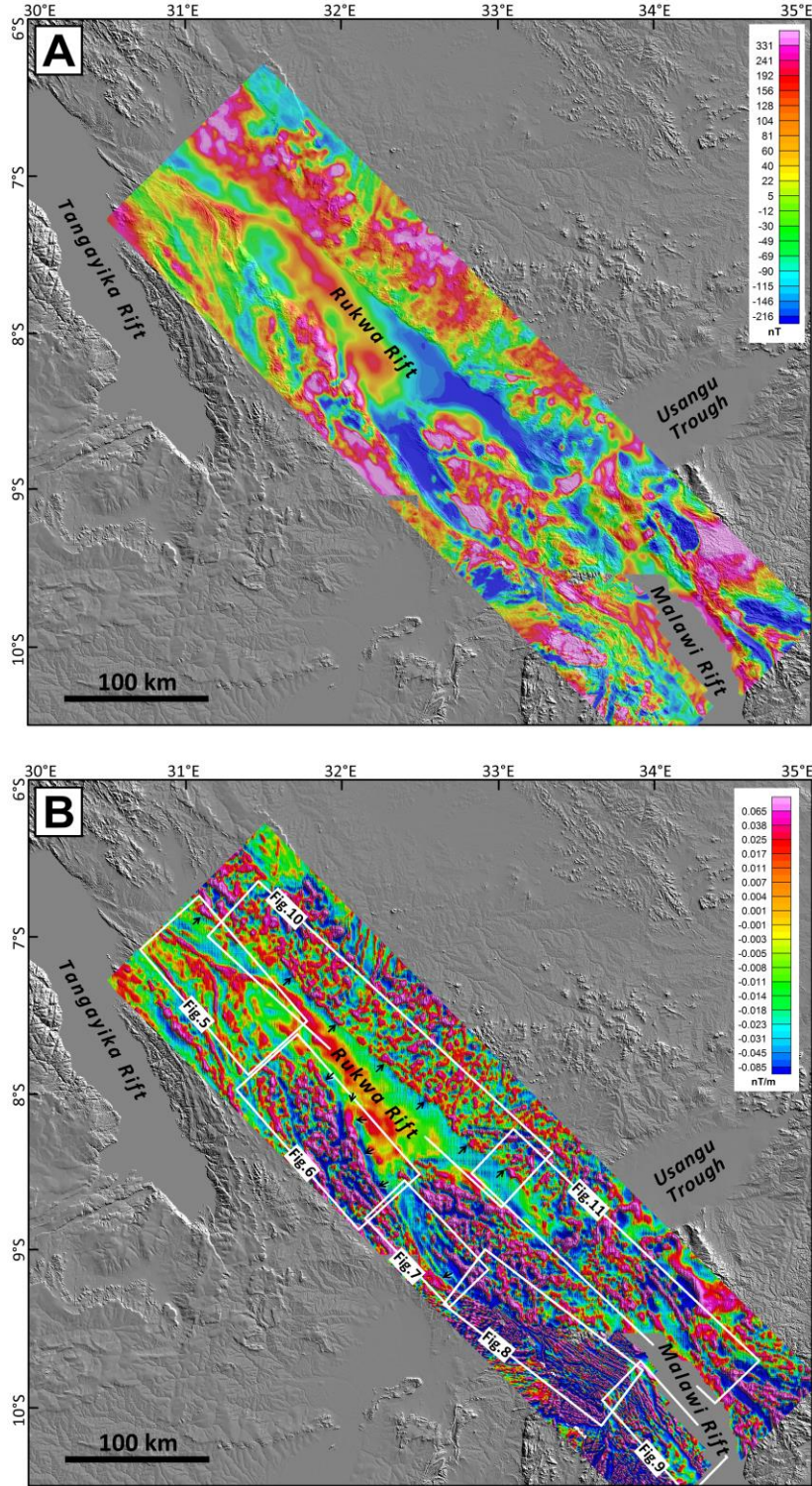
Fig. 4. (A) The reduced to pole Total Magnetic Intensity (RTP-TMI) map of the Rukwa-North Malawi Rift area, draped over the topographic digital elevation model of SW Tanzania. (B) The 1st vertical derivative map of the RTP-TMI map of the Rukwa-North Malawi Rift area draped over the topographic digital elevation model.

1211
1212
1213
1214
1215
1216
1217
1218
1219
1220
1221
1222
1223
1224
1225
1226
1227
1228
1229
1230
1231
1232
1233
1234
1235
1236
1237
1238
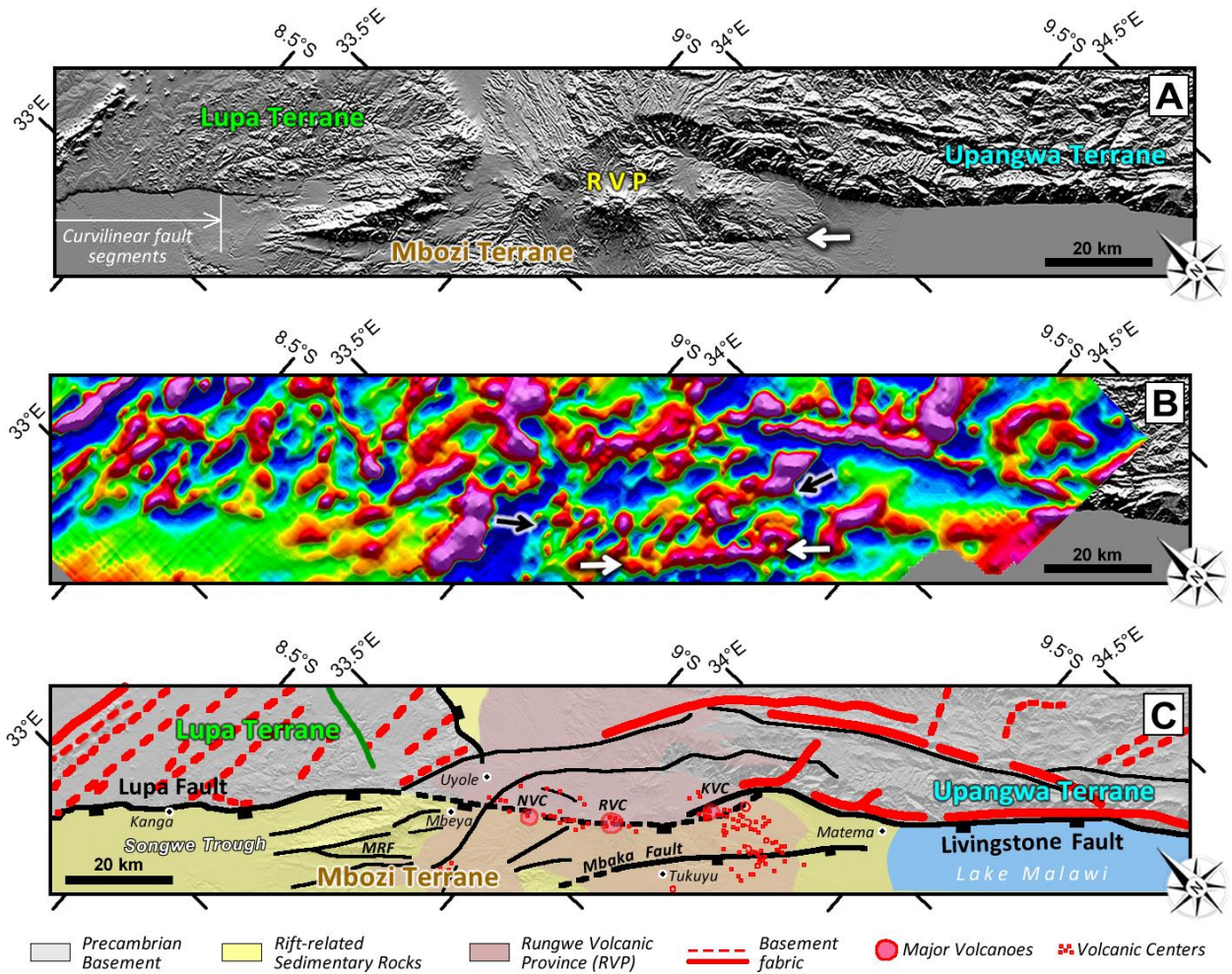1239
1240
1241
1242
1243
1244
1245
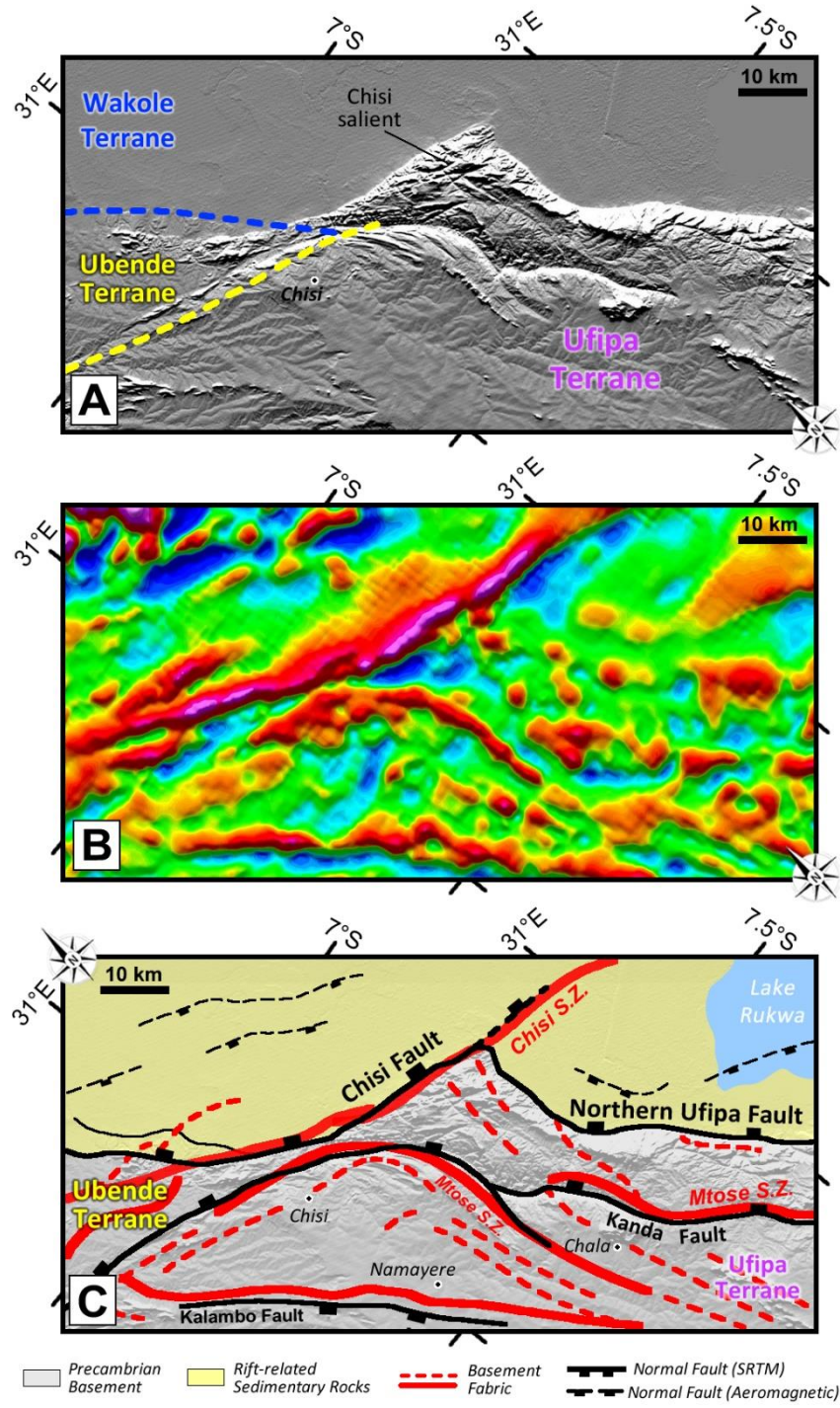
1246 Fig. 5. Northernmost part of the Ufipa Fault, the SW boundary fault of the Rukwa Rift.
1247 Topographic digital elevation model in the top panel (A), the vertical derivative of the magnetic
1248 data in the middle panel (B), and a structural interpretation in the bottom panel (C).

1249

1250
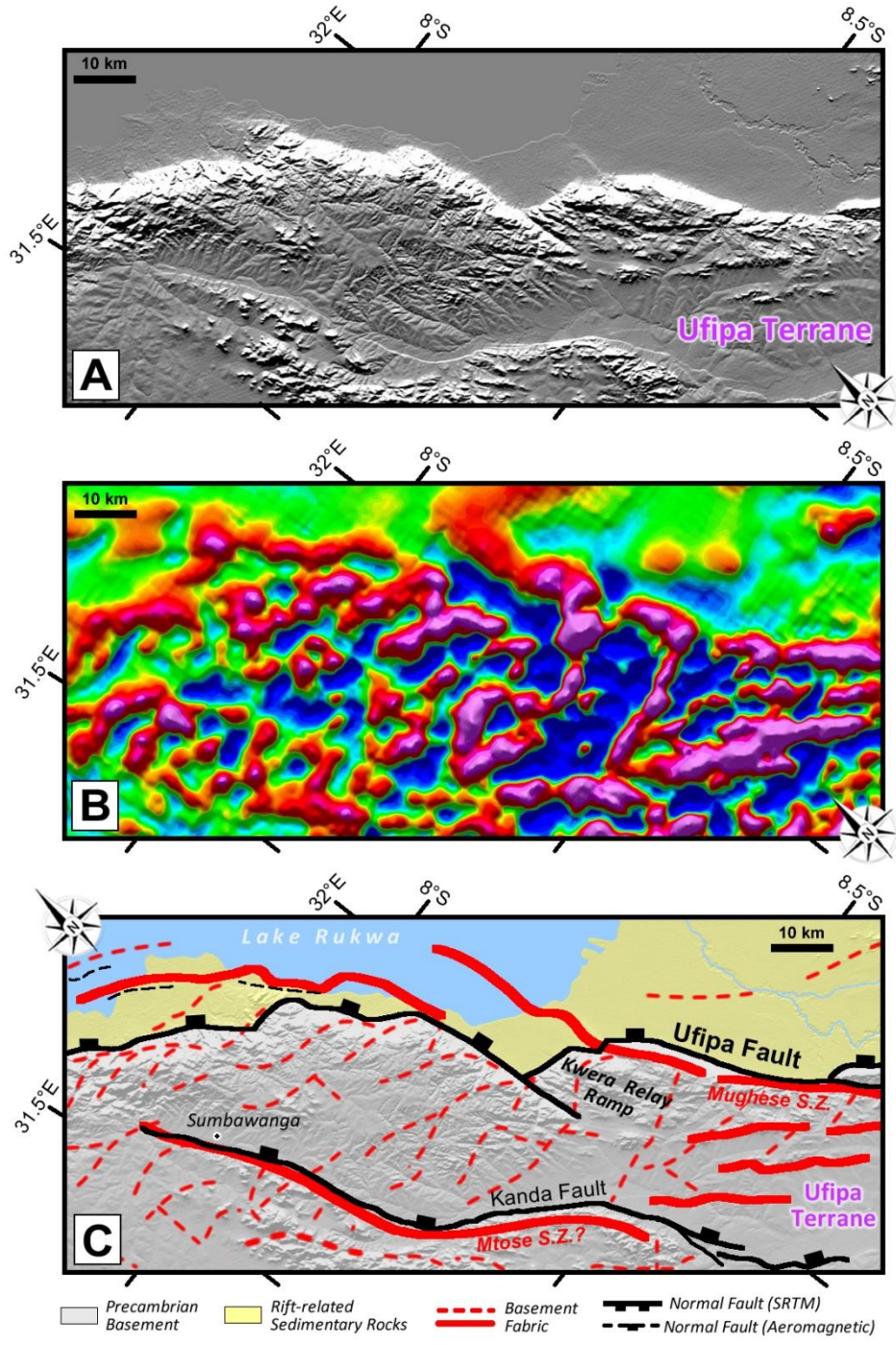
Fig. 6. Central segment of the Ufipa Fault, SW boundary of the Rukwa Rift. Topographic digital elevation model in the top panel (A), the vertical derivative of the magnetic data in the middle panel (B), and a structural interpretation in the bottom panel (C).
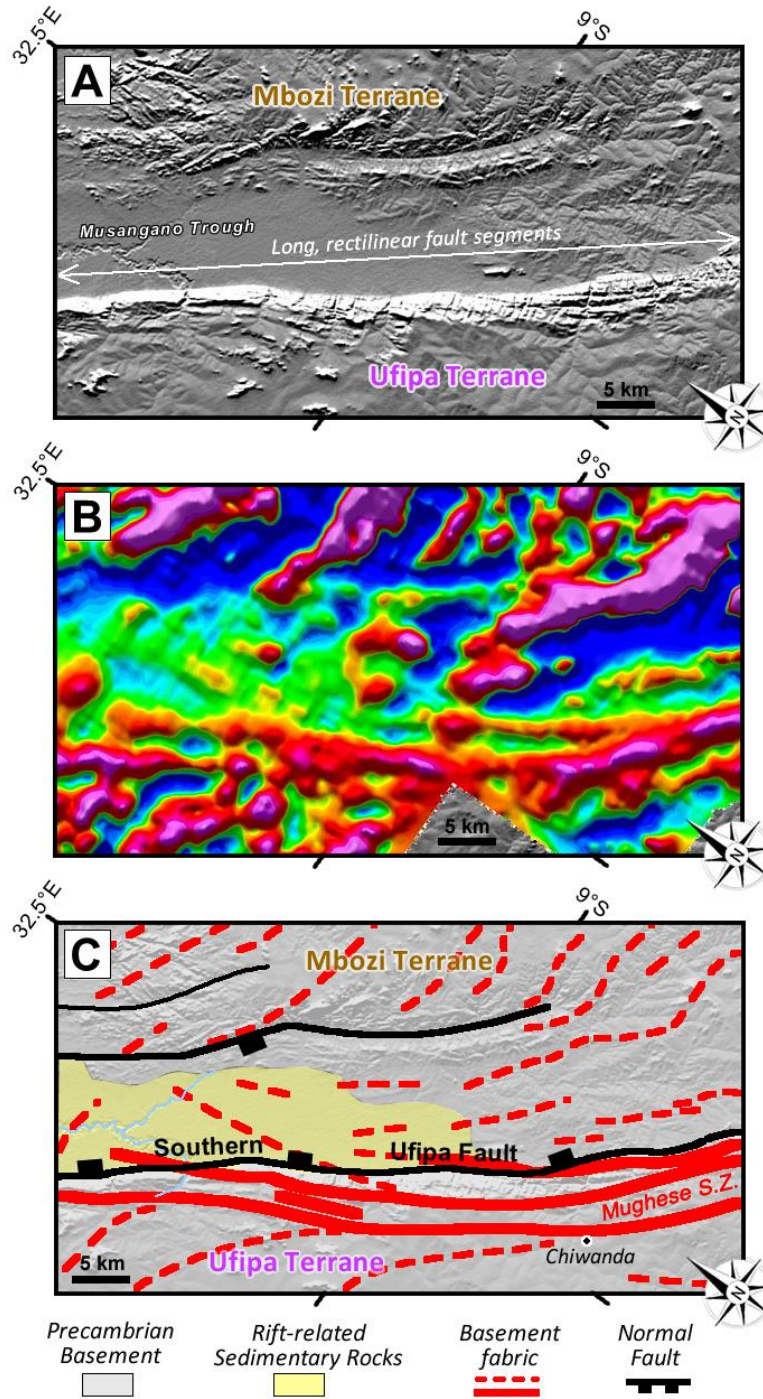
Fig. 7. The Musangano Trough part of the SW boundary of the Rukwa Rift. Topographic digital elevation model in the top panel (A), the vertical derivative of the magnetic data in the middle panel (B), and a structural interpretation in the bottom panel (C).
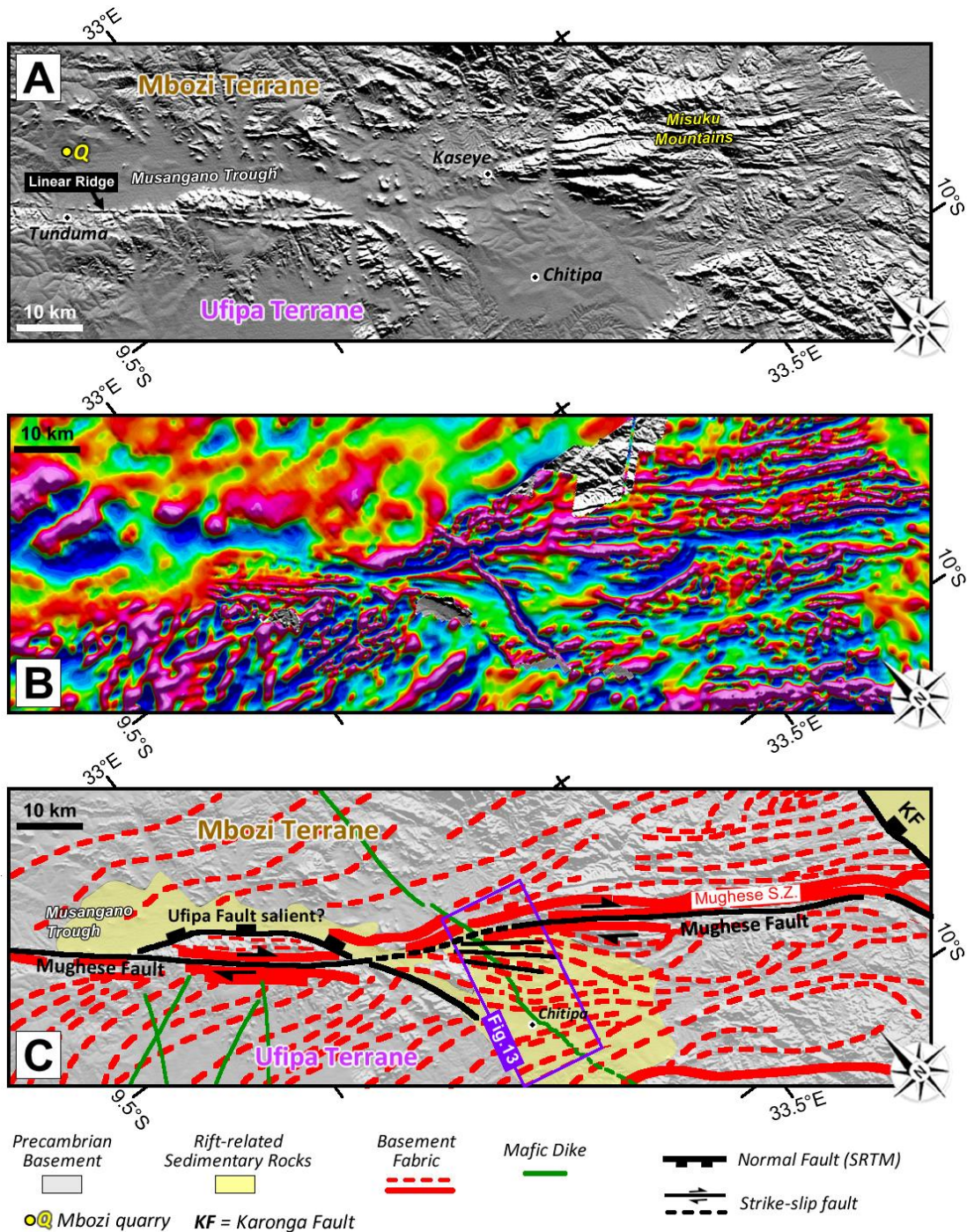
Fig. 8. The SW margin of the Mbozi Block. Topographic digital elevation model in the top panel (A), the vertical derivative of the magnetic data in the middle panel (B), and a structural interpretation in the bottom panel (C).
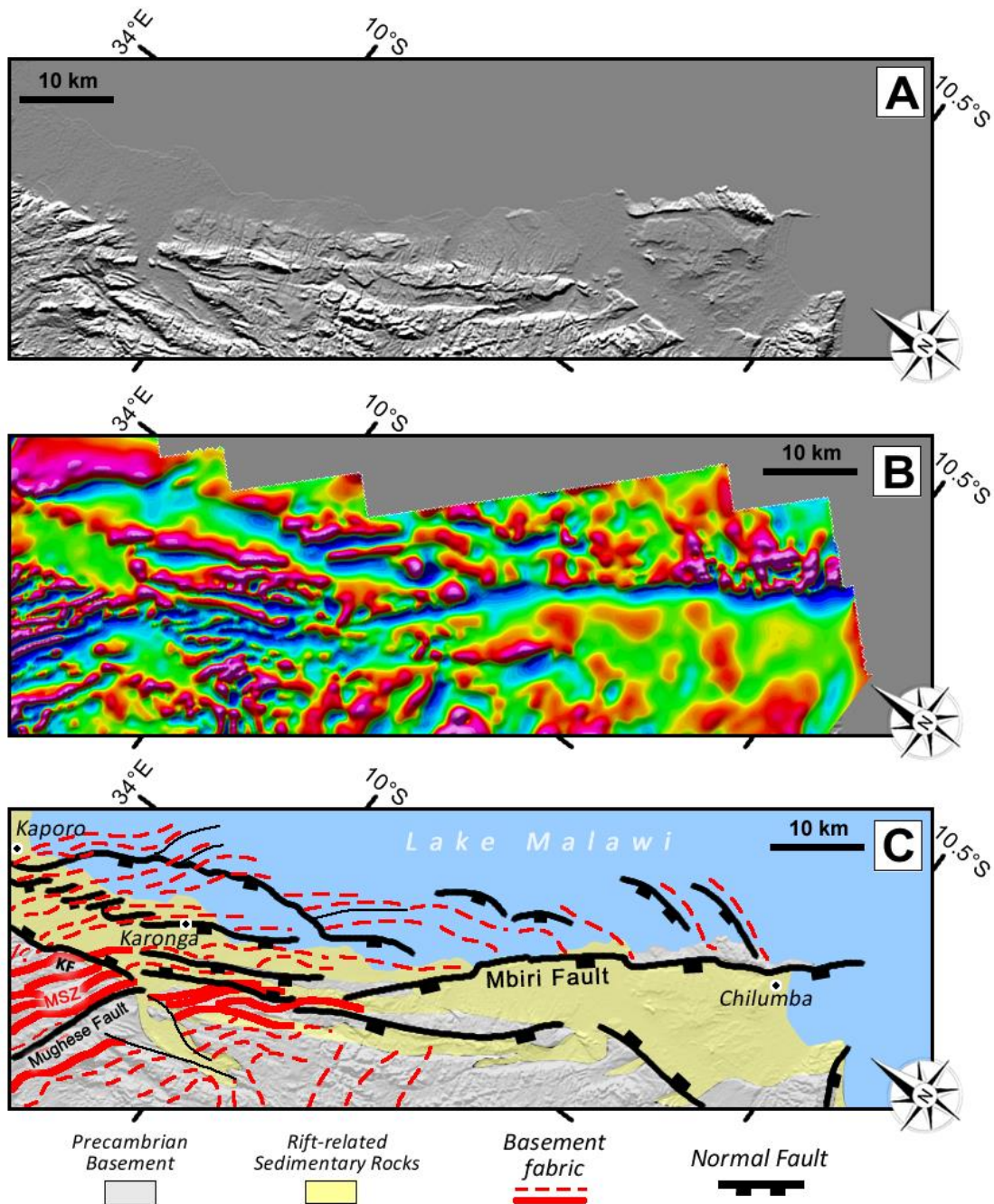
Fig. 9. The SW margin of the North Malawi Rift Basin (Karonga area). Topographic digital elevation model in the top panel (A), the vertical derivative of the magnetic data in the middle panel (B), and a structural interpretation in the bottom panel (C). MSZ = Mughese Shear Zone, KF = Karonga Fault. Fault and basement fabric interpretations from Kolawole et al. (2018).
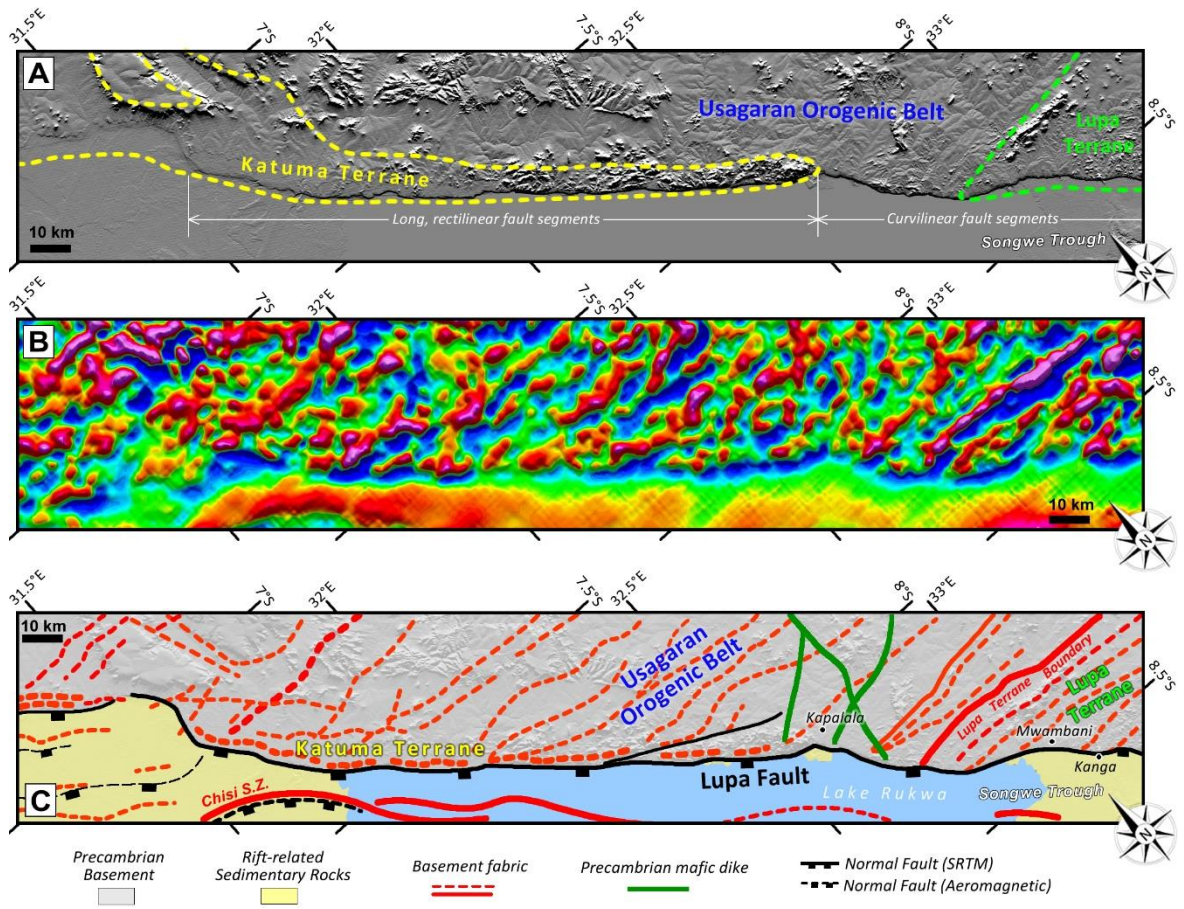
Fig. 10. The northern section of the Lupa Fault, the NE boundary fault of the Rukwa Rift. Topographic digital elevation model in the top panel (A), the vertical derivative of the magnetic data in the middle panel (B), and a structural interpretation in the bottom panel (C).

1446

Fig. 11. The southern section of the Lupa Fault, the NE margin of the Mbozi Block (Rungwe Volcanic Province) and a section of the Livingstone Fault (NE border fault if the North Malawi Rift. Topographic digital elevation model in the top panel (A), the vertical derivative of the magnetic data in the middle panel (B), and a structural interpretation in the bottom panel (C). KVC = Kyejo Volcanic Center; NVC = Ngozi Volcanic Center; RVC = Rungwe Volcanic Center. Volcanic centers from Fontijn et al. (2010, 2012).

1447
1448
1449
1450
1451
1452
1453
1454
1455
1456
1457
1458
1459
1460
1461
1462

1463
1464
1465
1466
1467
1468
1469
1470
1471
1472
1473
1474
1475
1476
1477
1478
1479
1480
1481
1482
1483
1484
1485
1486
1487
1488
1489
1490
1491
1492
1493
1494
1495
1496
1497
1498
1499
1500
1501
1502
1503
1504
1505
1506
1507
1508
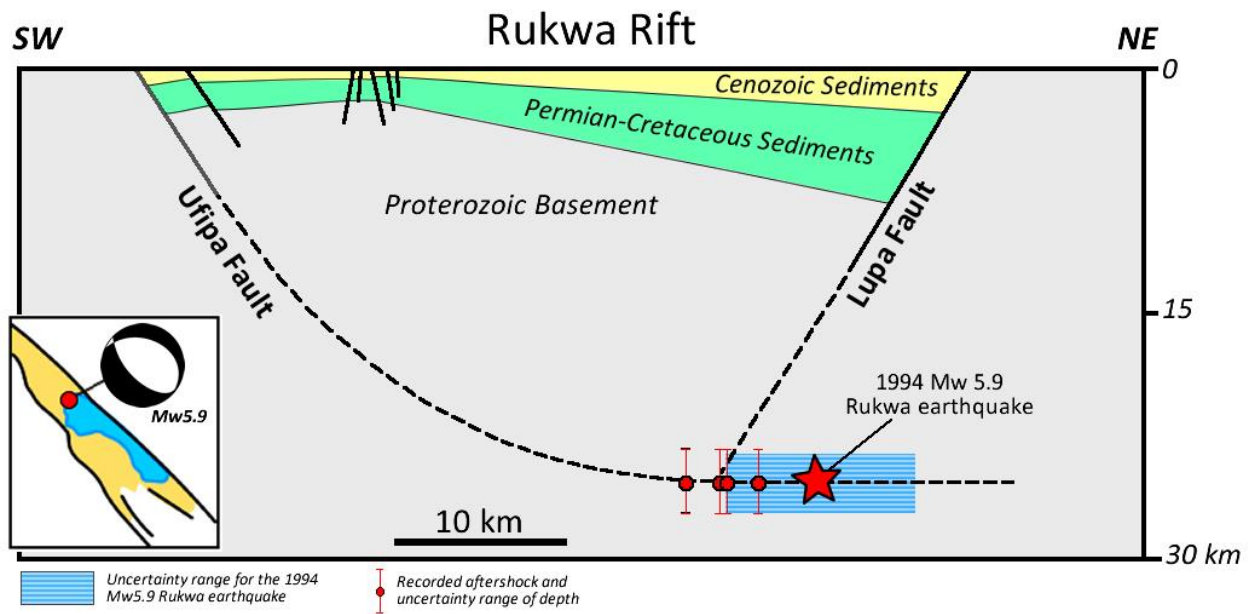
Fig. 12. Generalized geometrical relations of stratigraphic units and normal faults of the Rukwa rift, showing thickening of Cenozoic sediments towards both the Lupa and Ufipa border faults (modified after Zhao et al., 1997).
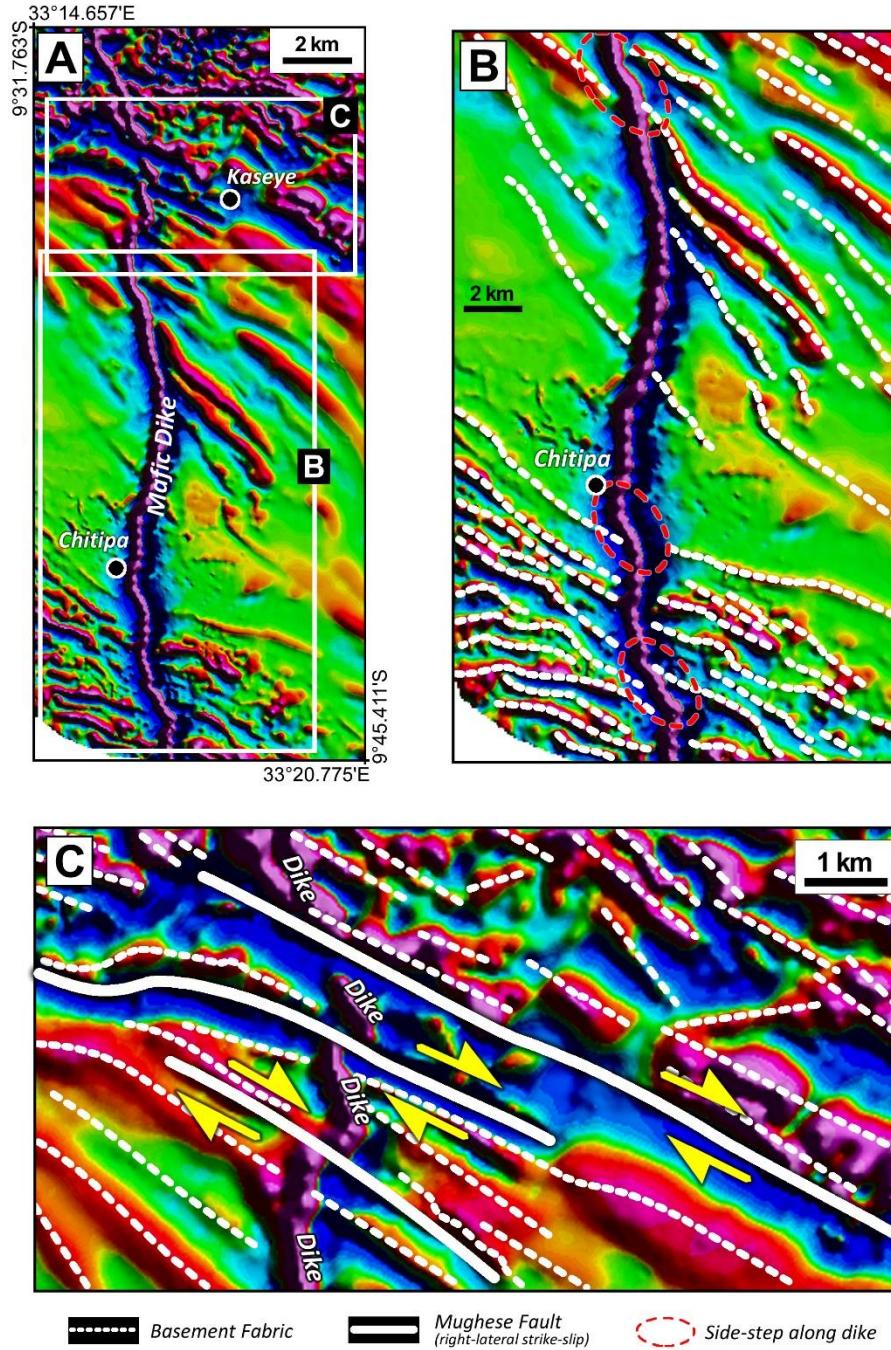
Fig. 13. (A) 1st vertical derivative of the aeromagnetic data covering the Kaseye-Chitipa area along the SW margin of the Mbozi Block (see location in Fig. 8C). (B) Close-up of the central and southern segments of a buried mafic dike (the "Chitipa Dike") showing side-stepping segments that coincide with pre-existing basement fabric. (C) Close-up of the northern segment of the dike showing right-lateral offsets by the continuation of the Ufipa Fault. This strike-slip fault segment is here-in referred to as the Mughese Fault.

1555
1556
1557
1558
1559
1560
1561
1562
1563
1564
1565
1566
1567
1568
1569
1570
1571
1572
1573
1574
1575
1576
1577
1578
1579
1580
1581
1582
1583
1584
1585
1586
1587
1588
1589
1590
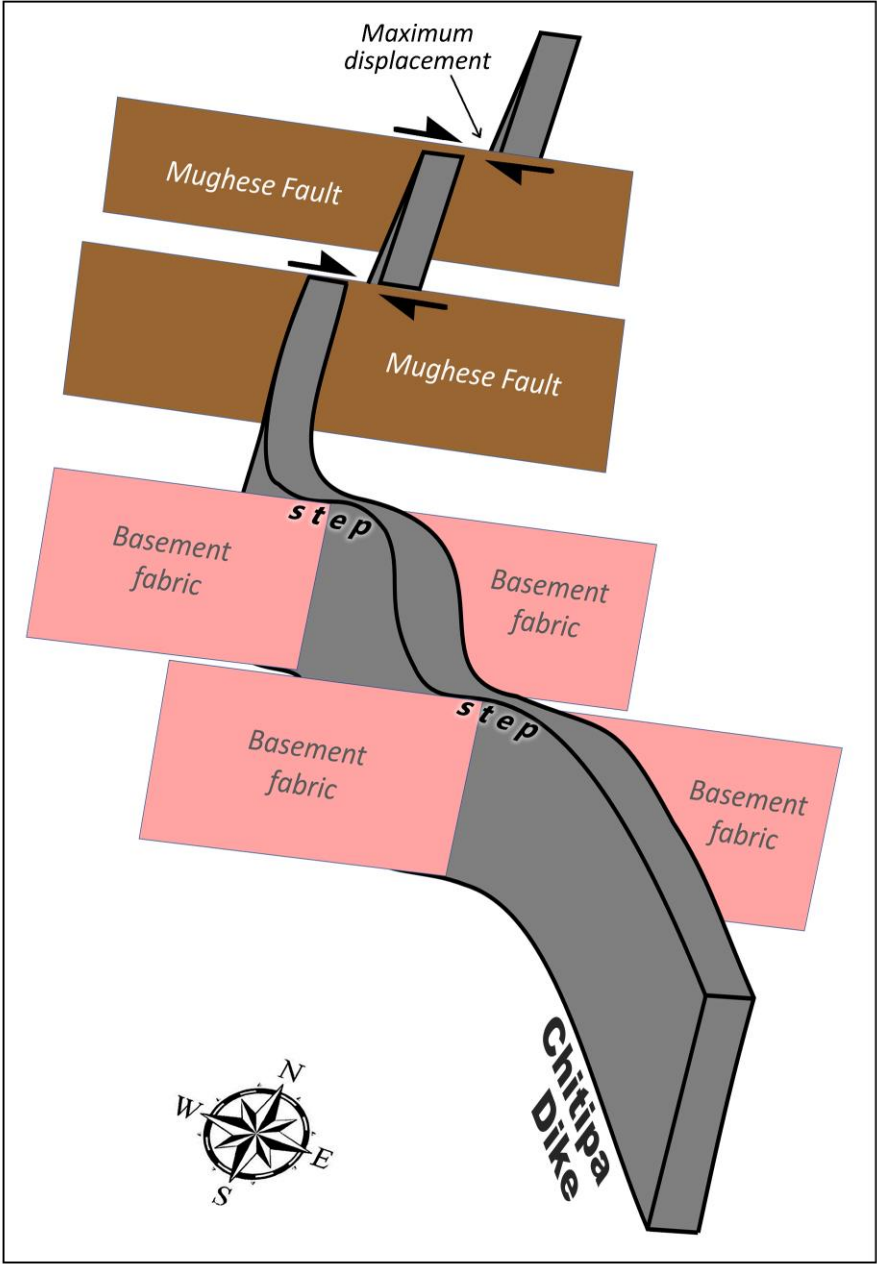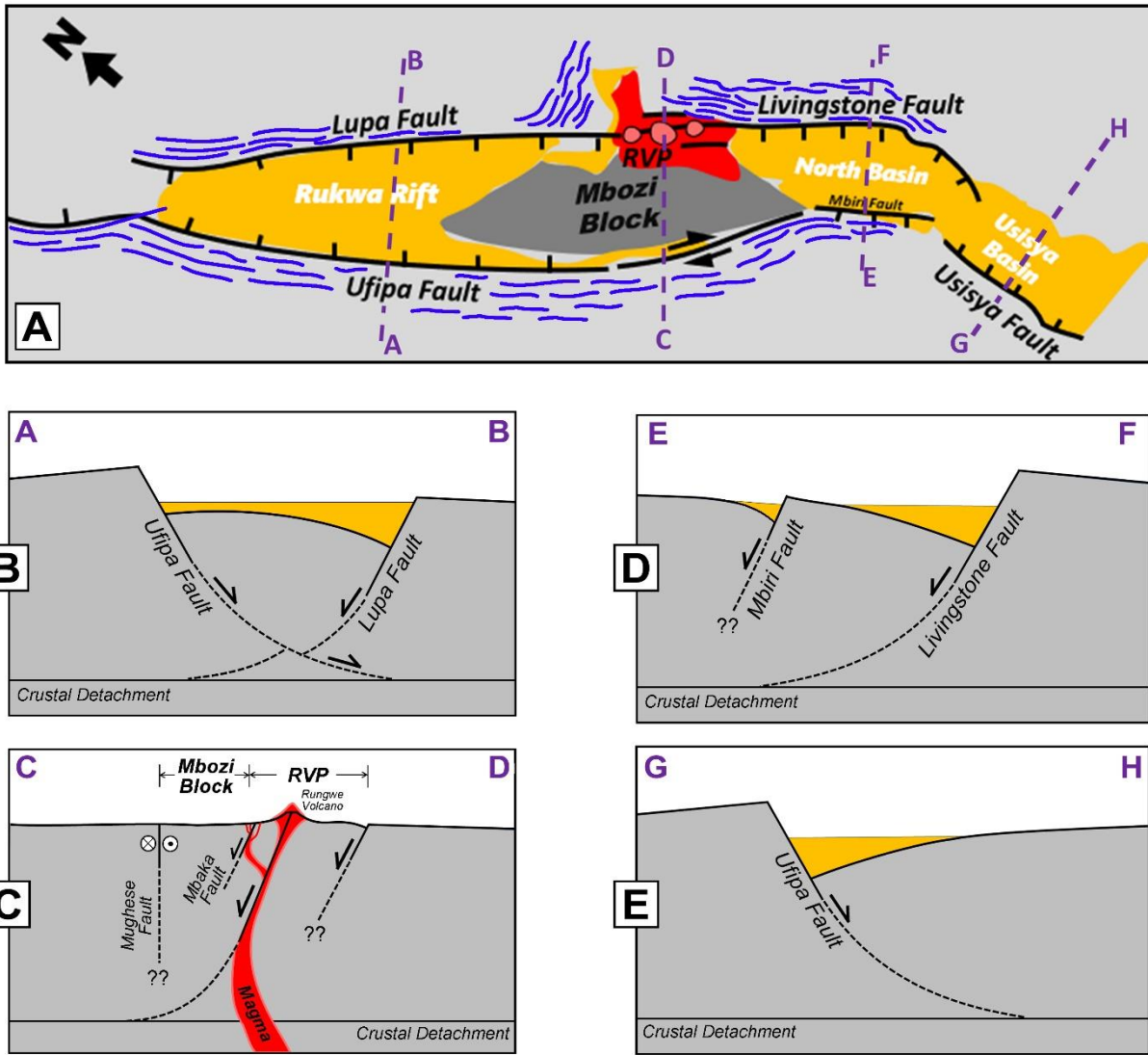1591
1592
1593
1594
1595
1596
1597
1598
1599
1600

Fig. 14. 3-dimensional (3-D) conceptual model of the geometry of the interpreted dike (the "Chitipa Dike") and its interactions with the pre-existing basement fabric and the post-emplacement Mughese strike-slip fault offset.
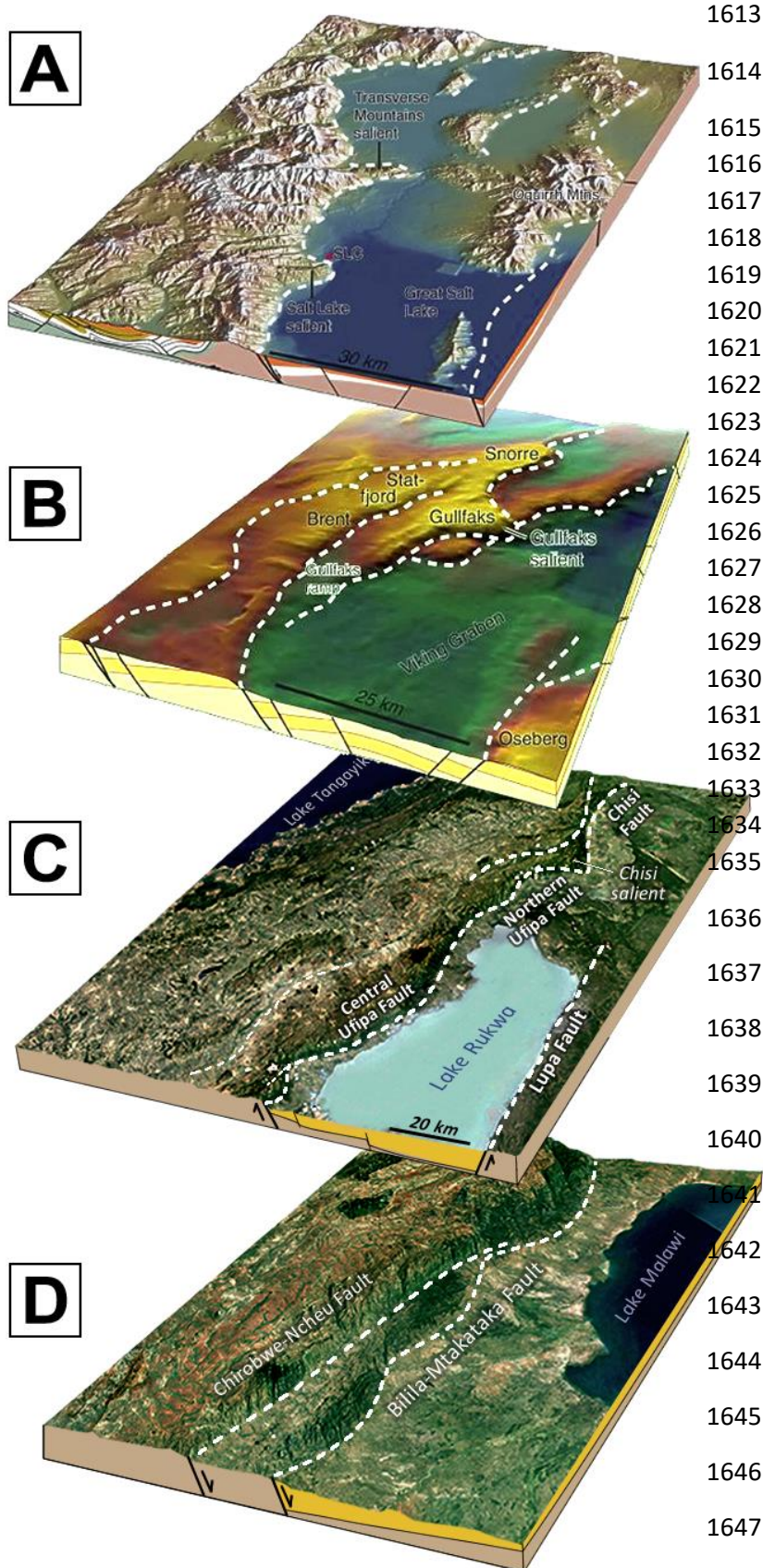
Fig. 15. (A) Generalized cartoon (map view) of the Rukwa-North Malawi Rift Segment (RNMRS) illustrating the continuous structural connectivity along the northeast and southwest boundaries, guided by the basement fabric. Black solid line = fault, blue solid line = basement fabric. RVP = Rungwe Volcanic Province. (B-E) Cross-section cartoons across the segments of the RNMRS, illustrating the possible subsurface geometries and interactions of the domain-bounding structures. LLF = Livingstone-Lupa Fault.

A

Transverse Mountains salient

Oquirrh Mtns

SLC

Salt Lake salient

Great Salt Lake

30 km

B

Snorre

Stat-fjord

Brent

Gullfaks

Gullfaks salient

Gullfaks fault

Viking Graben

Oseberg

25 km

C

Lake Tanganyika

Chisi Fault

Chisi salient

Northern Ufipa Fault

Central Ufipa Fault

Lake Rukwa

Lupa Fault

20 km

D

Chirobwe-Ncheu Fault

Bilila-Mtakataka Fault

Lake Malawi

Fig. 16. (A-B) The Wasatch Fault in the Salt Lake area, Utah, and the first-order faults in the northern North Sea (base Cretaceous unconformity) showing concave-curvilinear fault geometries (modified after Fossen and Rotevatn, 2016). (C) Strikingly similar Concave-curvilinear fault geometry occurs in the northern Ufipa Fault and Chisi Fault in the Rukwa Rift. However, the Central Ufipa Fault shows convex-curvilinear fault geometry. (D) The Bilila-Mtakataka Fault also shows excellent convex curvilinear fault geometries.
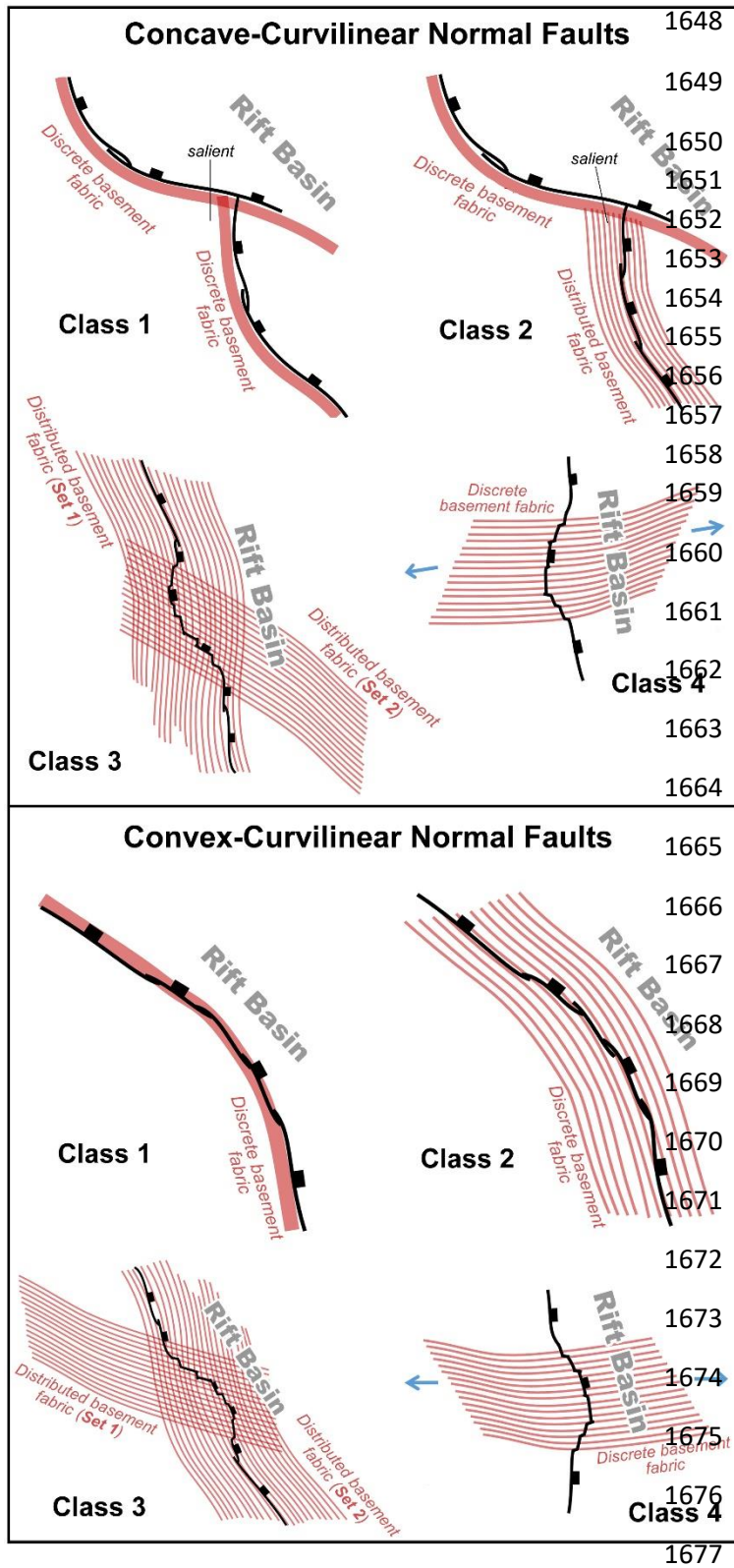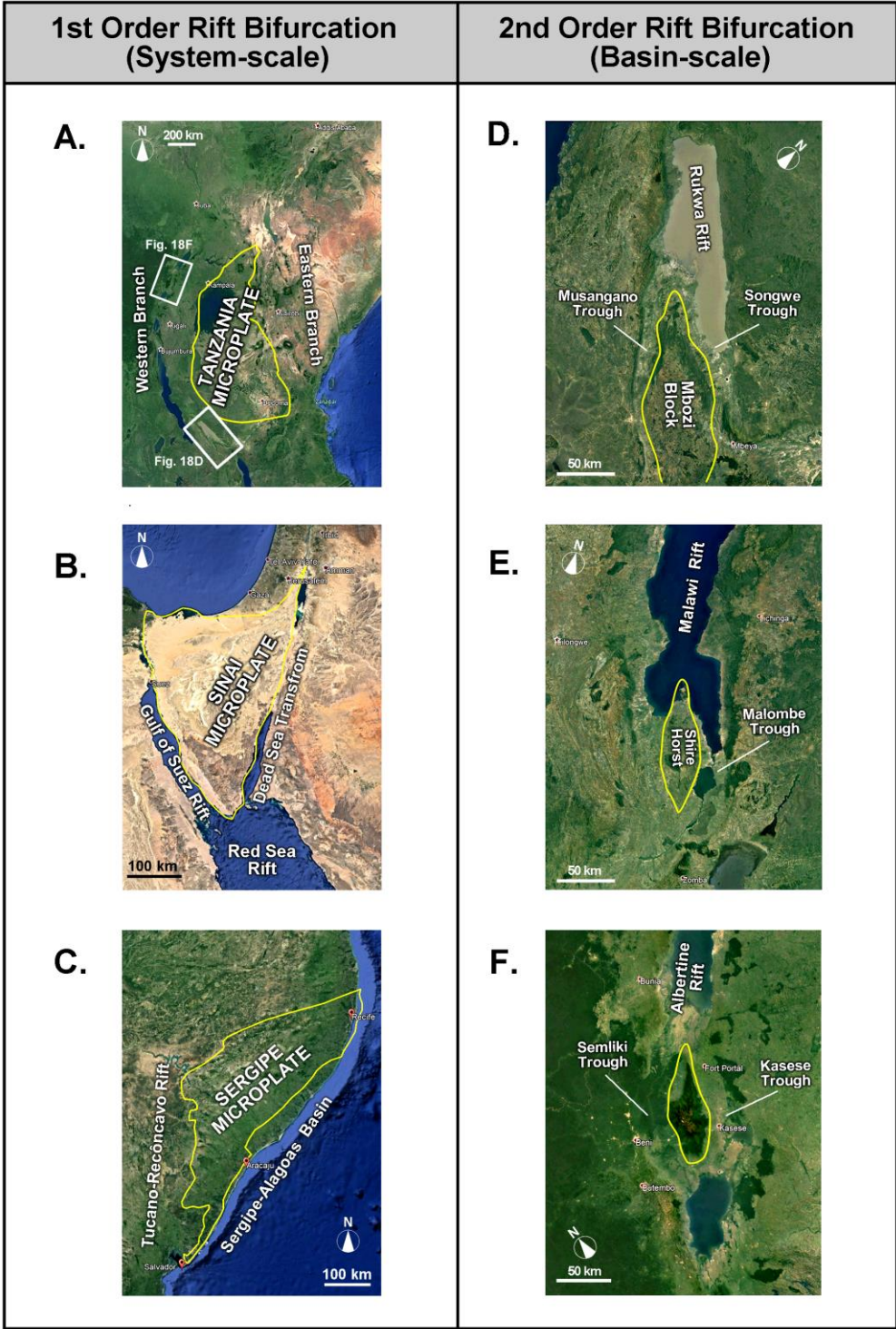
Fig. 17. Models illustrating the control of varying configurations of pre-existing basement fabrics on the development of concave- and convex-curvilinear normal fault plan-view geometries. These models are based on the observations from the Rukwa – North Malawi Rift Segment (this study).

1648
1649
1650
1651
1652
1653
1654
1655
1656
1657
1658
1659
1660
1661
1662
1663
1664
1665
1666
1667
1668
1669
1670
1671
1672
1673
1674
1675
1676
1677

1678

1679

Fig. 18. Examples of system-scale rift bifurcation in the (A) East African Rift System, (B) Red Sea Rift and (C) South Atlantic Rift; and examples of basin-scale rift bifurcation in the (D) Rukwa Rift (see Fig. 18A for location), (E) southern Malawi Rift and (F) Albertine Rift (see Fig. 18A for location). These examples show that the 2nd order bifurcations are integral components of inter-rift transfer zones where the coupling of rift segments take place.